OPEN ACCESS

African Journal of **Biotechnology**

3 April 2019
ISSN 1684-5315
DOI: 10.5897/AJB
www.academicjournals.org

ACADEMIC JOURNALS
expand your knowledge

About AJB

The African Journal of Biotechnology (AJB) is a peer reviewed journal which commenced publication in 2002. AJB publishes articles from all areas of biotechnology including medical and pharmaceutical biotechnology, molecular diagnostics, applied biochemistry, industrial microbiology, molecular biology, bioinformatics, genomics and proteomics, transcriptomics and genome editing, food and agricultural technologies, and metabolic engineering. Manuscripts on economic and ethical issues relating to biotechnology research are also considered.

Indexing

CAB Abstracts, CABI's Global Health Database, Chemical Abstracts (CAS Source Index) Dimensions Database, Google Scholar, Matrix of Information for The Analysis of Journals (MIAR), Microsoft Academic, Research Gate

Open Access Policy

Open Access is a publication model that enables the dissemination of research articles to the global community without restriction through the internet. All articles published under open access can be accessed by anyone with internet connection.

The African Journals of Biotechnology is an Open Access journal. Abstracts and full texts of all articles published in this journal are freely accessible to everyone immediately after publication without any form of restriction.

Article License

All articles published by African Journal of Biotechnology are licensed under the Creative Commons Attribution 4.0 International License. This permits anyone to copy, redistribute, remix, transmit and adapt the work provided the original work and source is appropriately cited. Citation should include the article DOI. The article license is displayed on the abstract page the following statement:

This article is published under the terms of the Creative Commons Attribution License 4.0
Please refer to https://creativecommons.org/licenses/by/4.0/legalcode for details
about Creative Commons Attribution License 4.0

Article Copyright

When an article is published by in the African Journal of Biotechnology, the author(s) of the article retain the copyright of article. Author(s) may republish the article as part of a book or other materials. When reusing a published article, author(s) should; Cite the original source of the publication when reusing the article. i.e. cite that the article was originally published in the African Journal of Biotechnology. Include the article DOI Accept that the article remains published by the African Journal of Biotechnology (except in occasion of a retraction of the article) The article is licensed under the Creative Commons Attribution 4.0 International License.

A copyright statement is stated in the abstract page of each article. The following statement is an example of a copyright statement on an abstract page.

Copyright ©2016 Author(s) retains the copyright of this article.

Self-Archiving Policy

The African Journal of Biotechnology is a RoMEO green journal. This permits authors to archive any version of their article they find most suitable, including the published version on their institutional repository and any other suitable website.

Please see http://www.sherpa.ac.uk/romeo/search.php?issn=1684-5315

Digital Archiving Policy

The African Journal of Biotechnology is committed to the long-term preservation of its content. All articles published by the journal are preserved by Portico. In addition, the journal encourages authors to archive the published version of their articles on their institutional repositories and as well as other appropriate websites.

https://www.portico.org/publishers/ajournals/

Metadata Harvesting

The African Journal of Biotechnology encourages metadata harvesting of all its content. The journal fully supports and implement the OAI version 2.0, which comes in a standard XML format. See Harvesting Parameter

Memberships and Standards

Academic Journals strongly supports the Open Access initiative. Abstracts and full texts of all articles published by Academic Journals are freely accessible to everyone immediately after publication.

Crossref is an association of scholarly publishers that developed Digital Object Identification (DOI) system for the unique identification published materials. Academic Journals is a member of Crossref and uses the DOI system. All articles published by Academic Journals are issued DOI.

Similarity Check powered by iThenticate is an initiative started by CrossRef to help its members actively engage in efforts to prevent scholarly and professional plagiarism. Academic Journals is a member of Similarity Check.

CrossRef Cited-by Linking (formerly Forward Linking) is a service that allows you to discover how your publications are being cited and to incorporate that information into your online publication platform. Academic Journals is a member of CrossRef Cited-by.

Academic Journals is a member of the International Digital Publishing Forum (IDPF). The IDPF is the global trade and standards organization dedicated to the development and promotion of electronic publishing and content consumption.

Contact

Editorial Office: ajb@academicjournals.org

Help Desk: helpdesk@academicjournals.org

Website: http://www.academicjournals.org/journal/AJB

Submit manuscript online http://ms.academicjournals.org

Academic Journals
73023 Victoria Island, Lagos, Nigeria
ICEA Building, 17th Floor,
Kenyatta Avenue, Nairobi, Kenya.

Editor-in-Chief

Editorial Board Members

Table of Content

Vol. 18(14), pp. 289-295, 3 April, 2019
DOI: 10.5897/AJB2018.16725
Article Number: 77AFE5A60591
ISSN: 1684-5315

http://www.academicjournals.org/AJB

ACADEMIC JOURNALS
expand your knowledge

African Journal of Biotechnology

Full Length Research Paper

Genetic diversity among *Fusarium* species associated with sorghum stalk rot in Southern Ethiopia

Alemayehu Chala

School of Plant and Horticultural Sciences, College of Agriculture, Hawassa University, P. O. Box 5, Hawassa, Ethiopia.

Received 6 December, 2018;Accepted 13 March, 2019

Fusaria are very diverse and destructive pathogens affecting different crops. However, their identity and diversity are unresolved in countries like Ethiopia, where various crop species are grown under differing environmental conditions. The objectives of this paper were to identify *Fusarium* spp. associated with sorghum stalk rot in Southern Ethiopia, and elucidate the genetic diversity within and between the species. For this purpose, Fusaria associated with sorghum from two locations in Southern Ethiopia were isolated. Sequencing of the elongation factor 1-alpha gene (EF-1α) was used for species identification. In addition, AFLP analysis was employed for further diversity studies within and between the *Fusarium* spp. Sequence analyses revealed the presence of two *Fusarium* spp. The first was identified as *Fusarium andiyazi*, while the identity of the second remains to be solved. AFLP analysis clustered the isolates into two major groups. The Dice similarity coefficients ranged from 0.39 to 0.91 for isolates of *F. andiyazi* while isolates within the new *Fusarium* spp. had a Dice similarity coefficient varying between 0.69 and 0.96. Cluster analysis and principal coordinate analysis clearly indicated a genetic separation between the two species. Both groups were pathogenic to mature sorghum plants following a toothpick inoculation test. More researches are required to identify the new species and elucidate the pathogenicity of the isolates.

Key words: EF-1α, *Fusarium andiyazi*, genetic similarity, sequence analysis, *Sorghum bicolor.*

INTRODUCTION

Sorghum (*Sorghum bicolor*, (L.) Moench) is the fifth most important cereal accounting for more than 65 million tons of annual production on over 45 million ha of land worldwide (FAO, 2017). The bulk of sorghum is produced in less developed nations (Berenji and Dahlberg, 2004), however, USA is the leading producer with more than 12 million tons of production (FAO, 2017). In Ethiopia, the crop is grown on more than 2 million ha of land making it one of the three most important crops both in terms of area coverage and total production (5 million tons) (CSA, 2018).

Sorghum is grown for its various purposes in different parts of the world. It serves as a major source of food and is also used as feed source for livestock especially in developed nations. In addition, sorghum is used as raw material for industries and for the production of bio-fuel. Despite its versatile use and ability to withstand adverse environmental conditions including moisture stress and

E-mail: alemayehuchala@yahoo.com. Tel: +251-(0)912-163096. Fax: +251-(0)46-2206711.

high temperatures, sorghum production is hampered by various biotic stresses among which diseases caused by different pathogens are one (Thakur and Mathur, 2000; Chala et al., 2011; 2012; Eshte et al., 2015). *Fusarium* species that cause stalk rot, ear rots and grain mold are among the major pathogens that infect sorghum (Frederiksen and Odvody, 2000; Leslie et al., 2005). The fungus *Fusarium* belongs to the most harmful pathogens of cultivated crops all over the world (Antonia, 1995; Ramdial et al., 2017).

Once they occur in the field or storage, *Fusaium* spp. are known to cause significant qualitative and quantitative yield reduction (Parry et al., 1995; Brandfass and Karlovsky, 2008). In addition, they produce mycotoxins that pose serious health risks to humans and animals that feed on contaminated grains (D'Mello et al., 1999; Pestka and Smolinsky, 2005; Antonissen et al., 2014; Wu et al., 2014 and Duan et al., 2016). Despite continued efforts to manage diseases caused by Fusaria, they still pose serious threats to grain producers across the world (Brandfass and Karlovsky, 2008). Since the early reports by Wollenweber and Reinking (1935), lots of researches have been conducted on the taxonomy/genetic diversity of the genus *Fusarium* (Summerell et al., 2011; O'Donnell et al., 2015; Laurence et al., 2016; Moussa et al., 2017 and Valente et al., 2017). However, research on *Fusarium* spp. from sorghum has been given only peripheral importance (Leslie et al., 2005). The only exceptions, in this regard, are earlier reports by Claflin (2000) and Leslie (2000; 2002), which identified more than 10 *Fusarium* species from sorghum, with many of them known to infect the stalk and grain. On the other hand, the identity and diversity of *Fusarium* species infecting sorghum in Africa, particularly in Ethiopia remains unresolved. In Ethiopia, there are limited reports (Ayalew, 2002; Ayalew et al., 2006; Chala et al., 2014; Taye et al., 2016; 2018) on *Fusarium* spp. and associated mycotoxins from sorghum even though the country is one of the primary centers of origin and diversity for the crop. The objectives of this work were: i) to identify *Fusarium* spp. associated with sorghum stalk rot in Southern Ethiopia; and ii) to elucidate the genetic diversity within and between the species.

MATERIALS AND METHODS

Isolate collection

Twenty sorghum stalks with visible rotting were randomly collected from sorghum fields in Southern Ethiopia during a routine field survey. The stalk samples were stored in paper bags at room temperature until isolation. Geographic description of the locations is given in Table 1.

Isolation, identification and storage of the isolates

Infected stalks were cut into pieces, surface sterilized using 0.5% sodium hypochlorite (NaOCl) solution for 90 s, and rinsed three times in sterile, distilled water. The cut and surface-sterilized stalks were placed on potato dextrose agar (PDA) and incubated at 25°C under continuous fluorescent light for 10 days. After 10 days of incubation, sporulation was observed in the PDA plates. Isolates were identified as Fusaria based on pigmentation and conidial morphology. On these bases, a total of 37 single spore isolates were transferred to new PDA plates. The isolates were grouped into two groups based on pigmentation and form of conidia. Pure cultures were maintained on potato dextrose agar (PDA) amended with 50 ppm of streptomycin, and stored at 4°C as stock cultures.

Molecular characterization

DNA extraction

Approximately 100 mg of fresh mycelium per isolate was crushed in liquid nitrogen using mortar and pestle. Fine powdered mycelium was transferred to a 2 ml microcentrifuge tube and genomic DNA was extracted using the DNeasy Plant Mini Kit (Qiagen Inc., Valencia, CA) following the manufacturer's instructions. The quality of the extracted DNA was controlled on 0.8% agarose gels and the DNA was stored at -20°C.

Species identification

Elongation factor 1-alpha genes of seven isolates, randomly selected from the two morphological groups, were partially sequenced using the EF-1α primers that is, EF-728F: 5´-CATCGAGAAGTTCGAGAAGG-3´ and EF-986R: 5´-TACTTGAAGGAACCCTTACC-3´ (Carbone and Kohn, 1999). The resulting sequences were BLAST searched with the NCBI nucleotide database for molecular species identification.

AFLP analysis

AFLP analysis was conducted following the method developed by Vos et al. (1995) with modifications that include the use of fluorescent labeled primers instead of radioactive labeled isotopes. Six combinations of *Mse*I and *Eco*RI primers were used for selective amplification (Table 2). The primers differ by two selective nucleotides at their 3´ ends and the *Eco*RI primers were labeled with the fluorescent dye FAM (6-carboxyfluorescein). The selective amplification reaction mix contained 1.6 µl dNTP (2.5 mM), 2 µl of 10× polymerase chain reaction (PCR) buffer, 0.08 µl of Taq DNA polymerase (5 U/µl), and 5 µl *Mse*I (6 ng/µl) and 1 µl *Eco*RI (1 pmol) primers to which 5 µl of 10 fold diluted preamplification PCR product was added as a template. The PCR amplification conditions were as follows: 1 cycle of 94°C for 30 s, 65°C for 30 s and 72°C for 60 s; 12 cycles where the annealing temperature was lowered by 0.7°C for each cycle; 23 cycles at 94°C for 30 s, 56°C for 30 s and 72°C for 60 s; finally 72°C for 7 min. The accuracy of the analysis was checked by running a randomly selected sample in duplicates.

Data scoring and analysis

Amplification products were separated in an ABI3730 DNA analyzer (Applied Biosystems Inc., Foster City, California) following the manufacturer's protocol and using GeneScan-1200 LIZ size standard (Applied Biosystems). The presence (1) and absence (0) of peaks were scored using Gene-Mapper software version 4.0 (Applied Biosystems Inc., Foster City, California), checked manually, and only clear and unambiguous peaks with fluorescence greater than or equal to 100 arbitrary units were entered into a binary data matrix for further analysis. The binary matrices were

Table 1. Geographic origin of *Fusarium* isolates.

Isolates	Origin	Altitude (m)	Latitude	Longitude
Fa_{1-16}	Welayita	1947-1952	6°58‘-6°60‘	37°51‘-37°53‘
Fsp_{1-22}	Gidole	1297-1590	5°40’-5°42’	37°22’-37°24’

then used to calculate genetic similarities between the isolates based on the Dice similarity coefficient (Dice, 1945), and the unweighted pair-group method with arithmetic average (UPGMA) was used to construct a genetic similarity tree with the help of the NTSYS-pc software, version 2.0 (Exeter Biological Software, Setauket, NY). To further elucidate the genetic relationship among the tested isolates, principal coordinate analysis was conducted using the software GenAlEx6 (Peakall and Smouse, 2006).

In-vitro growth rate of Fusarium isolates

To study the phenotypic characters (growth rate and colony morphology) of the *Fusarium* isolates, 5 mm portions of the 38 single spore isolates were transferred from the stock cultures and cultivated on PDA at 25°C in the dark. After five days of incubation, 3 mm mycelia plugs were taken from the actively growing edges of each isolate, transferred to the centre of four replicate PDA plates, and incubated in the dark at 25±2 and 30±2°C. For each isolate, radial growth was recorded at 24 h intervals for 7 days.

RESULTS

Species identification and characterization

Sequence analysis

Based on sequencing of the elongation factor 1-alpha gene (EF-1α) of isolates, the Fusaria were categorized into two groups. The first group of isolates were identified as *F. andiyazi*. The sequence of the second group of isolates did not match with the sequence of *Fusarium* species deposited in NCBI, and hence their identity remains to be resolved.

Morphological and cultural characterization

F. andiyazi isolates produced both macro- and micro-conidia and had a white mycelium that become some what pale through time. Isolates belonging to the unidentified *Fusarium* species also produced both micro- and macro- conidia on PDA while their mycelium consistently appeared white with a mass of orange colored spores. Isolates of similar morphological appearance were also obtained from sorghum and finger millet grains collected from different locations in Ethiopia (data not shown).

Isolates belonging to the two species also varied in terms of radial growth rate. The growth rate of isolates belonging to *F. andiyazi* ranged from 8 to 14 mm/day and 8 to 12 mm/day at 25±2 and 30±2°C, respectively. On the other hand, isolates belonging to the new species grew considerably faster (10-17 mm/day) at 25°C than at 30°C (7-12 mm/day). When five isolates representing *F. andiyazi* and 10 isolates from the new *Fusarium* species were used to inoculate the stalks of mature sorghum plants using the toothpick inoculation method (Cumagun et al., 2009), all of them produced typical lesions that were absent in the control plants. This suggested the pathogenicity of both species to sorghum and proved that they were responsible for the stalk rot of sorghum.

AFLP analysis

AFLP analysis of 38 isolates clustered them into two major groups (Figure 1). The first major group consists of 16 isolates identified as *F. andiyazi* by sequence analyses. Dice similarity coefficient for isolates belonging to this major group varied from 0.39 to 0.91 (Table 3). Results differentiated isolates of *F. andiyazi* into two sub-groups. The first sub-group consists of 7 isolates while the second sub-group is made of the remaining 9 isolates. The second major group consists of 22 isolates belonging to the unidentified *Fusarium* species and hence named as *Fusarium* spp. Isolates within this group had a Dice similarity coefficient ranging between 0.69 and 0.96, and hence they were considered as genetically more similar with one another than those within *F. andiyazi*, and likely represent a single species. One isolate within this group had 69% similarity while the rest had at least 70% similarty between each other. The six primer combinations used in this study generated a total of 200 clearly scorable bands. Of these, 71 (35.5%) were unique to the new *Fusarium* species while 70 bands (35%) were unique to *F. andiyazi* isolates. The remaining 59 bands (29.5%) were shared across the species. Of the 71 bands unique to *Fusarium* spp., 31 (56%) were polymorphic while 60 (86%) bands unique to *F. andiyazi* were also polymorphic.

Principal coordinates analysis (PCO) also revealed the population subdivision within and between the two *Fusarium* species. Accordingly, the isolates were categorized into three groups (Figure 2). The first three principal coordinates accounted for 89.4, 4.5 and 2.3% of the total variation, respectively. PCO grouped 16 of the *F. andiyazi* isolates that formed the first two clusters of the UPGMA tree into two groups. The first group was made of 9 isolates while the second PCO group consisted of 7

Table 2. Nucleotide sequences of adapters and primers used in the AFLP analysis.

Adapters	Primer sequences	Function
E*co*RI	5´CTCGTAGACTGCGTACC3´ CATCTGACGCATGGTTAA5´	Adapter
M*se*I	5´GACGATGAGTCCTGAG3´ TACTCAGGACTCAT5´	Adapter
E*co*RI	5´GACTGCGTACCAATTC3´	Nonselective primer
M*se*I	5´GATGAGTCCTGAGTAA3´	Nonselective primer

	Primer sequences	
Selective Primer combination	**E*co*RI (5´→3´)**	**MseI (5´→3´)**
E12 × M16	GAC-TGC-GTA-CCA-ATT-CAC	GAT-GAG-TCC-TGA-GTA-ACC
E19 × M15	GAC-TGC-GTA-CCA-ATT-CGA	GAT-GAG-TCC-TGA-GTA-ACA
E19 × M16	GAC-TGC-GTA-CCA-ATT-CGA	GAT-GAG-TCC-TGA-GTA-ACC
E20 × M17	GAC-TGC-GTA-CCA-ATT-CGC	GAT-GAG-TCC-TGA-GTA-ACG
E21 × M16	GAC-TGC-GTA-CCA-ATT-CGG	GAT-GAG-TCC-TGA-GTA-ACC
E21 × M17	GAC-TGC-GTA-CCA-ATT-CGG	GAT-GAG-TCC-TGA-GTA-ACG

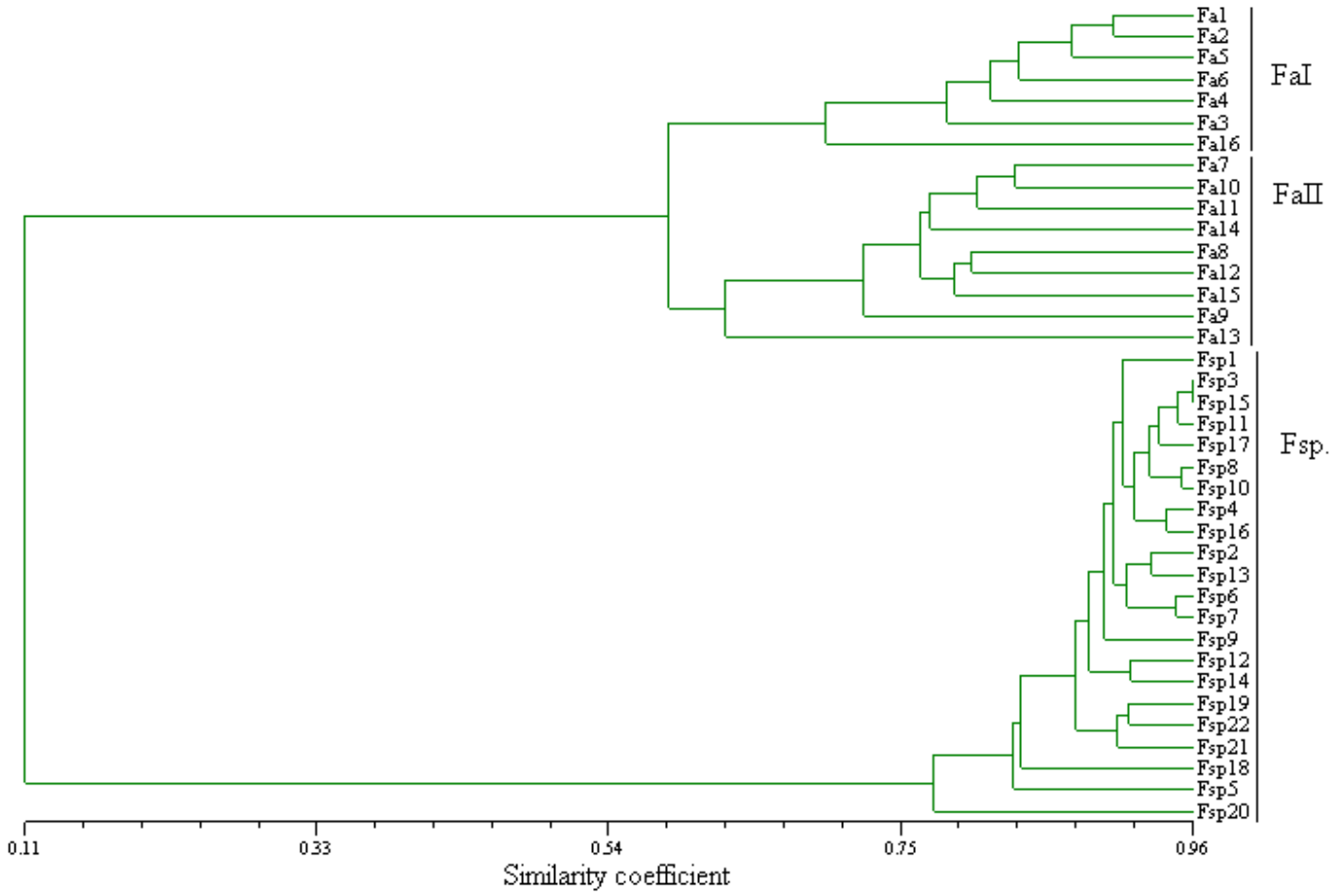

Figure 1. Dendogram showing the genetic diversity of 38 isolates of two *Fusarium* species based on Dice similarity matrix of AFLP bands.

Table 3. Dice similarity index within and between *Fusarium* species.

Species	*F. andyazi*	*Fusarium* spp.
Fusarium andyazi	0.391 - 0.907	0.044 - 0.227
Fusarium spp.	0.044 - 0.227	0.693 - 0.957

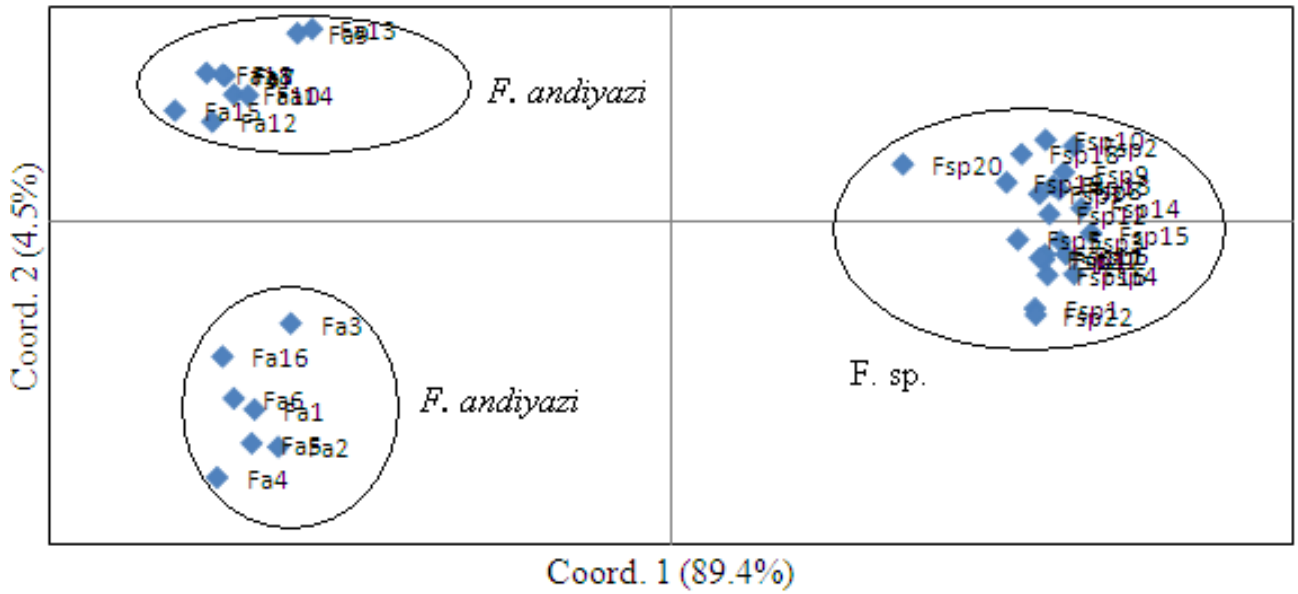

Figure 2. Principal coordinates analysis of 38 *Fusarium* isolates based on AFLP fingerprints.

isolates. The 22 remaining isolates belonging to the new *Fusarium* species were aggregated within a single PCO group with only 1 isolate barely separated from the rest. These results are in line with the cluster analysis of UPGMA.

DISCUSSION

The *Fusarium* isolates included in the current study fullfilled the morphological characteristics of *Fusarium* as described in Leslie and Summerell (2006). However, sequence analysis revealed the presence of two *Fusarium* species associated with stalk rot in Southern Ethiopia. The current results are in line with previous works that reported the co-occurence of different *Fusarium* spp. on the same plant (Summerell et al., 2011; Ramdial et al., 2017; Minnaar-Ontong et al., 2017). Results from sequencing confirmed the first species as *F. andiyazi*, a species which was first described by Marasas et al. (2001). This species was subsequently reported to be present in different parts of the world including Australia, Ethiopia, Nigeria, South Africa and United States (Marasas et al., 2001; Marley et al., 2004; Leslie et al., 2005; Leslie and Summerell, 2006 and Summerell et al., 2011). Nevertheless, except for initial reports, no further work has been done on this particular species in Ethiopia to the best of the author's knowledge. As a result, the diversity of this pathogen remains largely unknown to date.

Isolates belonging to the two *Fusarium* species varied not only in terms of their morphology and sequence but they also differed in growth rate, when incubated at 25 and 30°C. Isolates of *F. andiyazi* grew slower than those of the newly recovered *Fusarium* species at both temperatures. Besides, the growth rate of *F. andiyazi* isolates was also consistent across temperatures. Isolates of the same species showed similar growth rate at both of these temperatures in a previous study (Leslie et al., 2005). Isolates of *Fusarium* species on the other hand did not grow consistently across temperatures.

Although cultural/morphological characterizations provide a basis for both inter- and intra-species diversity studies; as suggested in other pathosystems, they may be unstable, highly influenced by the growth environments and rather change with the age of the colonies (Browning et al., 1999; Crouch et al., 2006 and Rivera-Vargas et al., 2006). As a result, such taxonomic features need to be supplemented with other characters like molecular markers that differentiate biological entities at the genetic level. Currently there is a growing

interest to assess the genetic diversity of fungi including Fusaria based on sequence analysis (McDonald et al., 2012; Leavitt et al., 2013; Maphosa et al., 2016; Laraba et al., 2017).

In accordance with sequence analysis and morpho-cultural characterization, AFLP analysis also showed the presence of at least two genetically distinct *Fusarium* populations associated with sorghum stalk rot in Southern Ethiopia. The two *Fusarium* species were not only genetically but also geographically separated as there is more than 50 km distance between the districts from where they were obtained. Backhouse et al. (2001) and Saremi et al., (1999) have reported climatic preferences among *Fusarium* species from both natural and agricultural ecosystems. This report was also supported by Vigier et al., (1997); De Wolf et al., (2003) and Moschini et al. (2004) that ascertained the influence of climate and local weather variations on the recovery of *Fusarium* species. Both UPGMA and PCO analyses of AFLP bands suggested greater variation within *F. andiyazi* than within *Fusarium* species. Leslie et al. (2005) proposed a 40% similarity cut-off to identify strains into a single species. As the most distantly related isolates within this species had a 39% Dice similarity, which is just close to the 40% boundary, it is better not to reach a conclusion that *F. andiyazi* isolates belong to different species.

In the current study, all isolates belonging to *F. andiyazi* were isolated from sorghum stalks collected from the district of Welayita, with elevation ranging from 1947 to 1952 m above sea level (masl), while those belonging to the new *Fusarium* species were isolated from the Gidole district, with elevation of 1297-1590 masl. Based on eleven years weather data from the National Meteorological Agency, Welayita district has a total annual rainfall of 1262 mm, and temperature of 13.6 - 23.4°C (18.5°C average). There is no reliable weather data for Gidole district. However, this relatively low lying district is known to have a more warm and humid weather than Welayita. Preparations are now underway to work on the speciation of isolates belonging to the new species, and to further characterize them on the basis of mycotoxin profiling, mating types and other characteristic features. *F. andyiazi* is not a known mycotoxin producer (Leslie et al., 2005). However, the toxin production potential of isolates belonging to the new *Fusarium* species need to be ascertained especially in light of their isolation from cereal grains. This is of paramount importance as several *Fusarium* spp. are known producers of mycotoxins that pose health risks to consumers of contaminated plant products (Antonissen et al., 2014; Wu et al., 2014; Van der Lee et al., 2015; Duan et al., 2016).

CONFLICT OF INTERESTS

The author has not declared any conflict of interests.

ACKNOWLEDGEMENT

The author apprieciates the Norwegian Agency for Development Cooperation (NORAD) for sponsoring the research through the CSA-NORHED project.

REFERENCES

Antonia S (1995). The occurrence and biology of some *Fusarium* spp., on wheat in Slovakia. Institute of Experimental Phytopathology and Entomology. Slovak Academy of Sciences, Ivanka pri Dunaji, Slovakia. 119 p.

Antonissen G, Martel An, Pasmans F, Ducatelle R, Verbrugghe E, Vandenbroucke V, Li S, Haesebrouck F, Immerseel FV, Croubels S (2014). The impact of Fusarium mycotoxins on human and animal host susceptibility to infectious diseases. Toxins 6:430-52.

Ayalew A (2002). Mycoflora and mycotoxins of major cereal grains and antifungal effects of selected medicinal plants from Ethiopia. Ph.D. Dissertation]. Goettingen, Germany: Georg August University.

Ayalew A, Fehrmann H, Lepschy J, Beck R, Abate D (2006). Natural occurrence of mycotoxins in staple cereals from Ethiopia. Mycopathologia 162:57-63.

Backhouse D, Burgess LW, Summerell BA (2001). Biogeography of *Fusarium*, p. 122-137. In: Summerell BA, Leslie JF, Backhouse D, Bryden WL, Burgess LW. (Eds.), Fusarium*:* Paul E. Nelson Memorial Symposium. APS Press, St. Paul, Minnesota.

Berenji J, Dahlberg J (2004). Perspectives of sorghum in Europe. Journal of Agronomy and Crop Science 190(5):332-338.

Brandfass C, Karlovsky P (2008). Upscaled CTAB-Based DNA Extraction and Real-Time PCR Assays for *Fusarium culmorum* and *F. graminearum* DNA in Plant Material with Reduced Sampling Error. International Journal of Molecular Sciences 9(11):2306-2321.

Browning M, Rowley LV, Zang P, Chandlee JM, Jackson N (1999). Morphological, pathogenic and genetic comparisons of *Colletotrichum graminicola* isolates from Poaceae. Plant Disease 83(3):286-92.

Chala A, Tronsmo AM, Brurberg MB (2011). Genetic differentiation and gene flow in *Colletotrichum sublineolum* in Ethiopia, the centre of origin and diversity of sorghum, as revealed by AFLP analysis. Plant Pathology 60(3):474-482.

Chala A, Tronsmo AM (2012). Evaluation of Ethiopian sorghum accessions for resistance against *Colletotrichum sublineolum*. European Journal of Plant Pathology 132(2):179-189.

Chala A, Taye W, Ayalew A, Krska R, Sulyok M, Logrieco A (2014). Multimycotoxin analysis of sorghum (*Sorghum bicolor* L. Moench) and finger millet (*Eleusine coracana* L. Garten) from Ethiopia. Food Control 45:29-35.

Claflin LE (2000). Fusarium root and stalk rot. In: Frederiksen RA, Odvody GN (eds.). Compendium of Sorghum Diseases. The American Phytopathology Society. St. Paula MN USA. pp 29-30.

Crouch JA, Clarke BB and Hillman BI (2006). Unraveling evolutionary relationships among divergent lineages of *Colletotrichum* causing anthracnose disease in turfgrass and corn. Phytopathology 96(1):46-60.

Central Statistical Agency (CSA) (2018). Agricultural Sampling Survey. Report on area and production of crops. http://www.csa.gov.et. Accessed February 2019.

Cumagun CJR, Ramos JS, Dimaano AO, Munaut F, Van Hove F (2009). Genetic characterization of *Fusarium verticilloides* from corn in the Philippines. Journal of General Plant Pathology 75:405-412.

Dice LR (1945). Measures of the amount of ecologic association between species. Ecology 26(3):297-302.

D'Mello JPF, Placinta CM, Macdonald AMC (1999). Fusarium mycotoxins: A review of global implications for animal health, welfare and productivity. Animal Feed Science and Technology 80(3-4):183-205.

De Wolf ED, Madden LV, Lipps PE (2003). Risk assessment models for wheat Fusarium head blight epidemics based on within-season weather data. Phytopathology 93(4):428-435.

Duan C, Qin Z, Yang Z, Li W, Sun S, Zhu Z, Wang X (2016). Identification of pathogenic *Fusarium* spp. causing maize ear rot and potential mycotoxin production in China. Toxins 8(6):186. doi: 10.3390/toxins8060186.

Eshte Y, Mitiku M, Shiferaw W (2015). Assessment of important plant disease of major crops (Sorghum, Maize, Common Bean, Coffee, Mung bean, Cowpea) in south Omo and Segen Peoples Zone of Ethiopia. Current Agriculture Research Journal 3(1):75-79 doi : http://dx.doi.org/10.12944/CARJ.3.1.10

Food and Agriculture Organization of the United Nations (FAO) (2017). FAOSTAT-Crop production data. http://faostat.fao.org. Accessed February 2019.

Frederiksen RA, Odvody GN (2000). Compendium of Sorghum Diseases. 2nd ed. The American Phytopathological Society, St. Paul, MN.

Laurence MH, Walsh JL, Shuttleworth LA, Robinson DM, Johansen RM, Petrovic T, Vu TTH, Burgess LW, Summerell BA, Liew ECY (2016). Six novel species of Fusarium from natural ecosystems in Australia. Fungal Diversity77(1):349-66.

Laraba I, Boureghda H, Abdallah A, Bouaicha O, Obanor F, Moretti A, Geiser DM, Kim HS, McCormick SP, Proctor RH, Kelly AC, Ward TJ, O'Donnell K (2017). Population genetic structure and mycotoxin potential of the wheat crown rot and head blight pathogen *Fusarium culmorum* in Algeria. Fungal Genetics and Biology 103:34-41.

Leavitt SD, Esslinger TL, Spribille T, Divakar PK, Thorsten LH (2013). Multilocus phylogeny of the lichen-forming fungal genus Melanohalea (Parmeliaceae, Ascomycota): insights on diversity, distributions, and a comparison of species tree and concatenated topologies. Molecular Phylogenetics and Evolution 66(1):138-152.

Leslie JF, Zeller KA, Lamprecht SC, Rheeder JP, Marasas WFO (2005). Toxicity, pathogenicity, and genetic differentiation of five species of *Fusarium* from sorghum and millet. Phytopathology 95(3):275-283.

Leslie JF (2000). *Fusarium* species associated with sorghum. In: Frederiksen RA, Odvody GN. (eds.). Compendium of Sorghum Diseases. The American Phytopathology Society. St. Paula. MN. USA P 30.

Leslie JF (2002). Sorghum and pearl millet diseases in the horn of Africa. In: Leslie JF (ed.). Sorghum and millet diseases. Blackwell publishing. Iowa State Press pp. 383-387.

Leslie JF, Summerell BA (2006). The Fusarium laboratory manual. Blackwell, IA, P 388.

Maphosa MN, Steenkamp ET, Wingfield BD (2016). Genome-based selection and characterization of *Fusarium circinatum*-specific sequences. G3 (Bethesda) 6(3):631-639.

Marasas WFO, Rheeder JP, Lamprecht SC, Zeller KA, Leslie JF (2001). *Fusarium andiyazi* sp. nov., a new species from sorghum. Mycologia 93(6):1203-1210.

Marley P, Marasas WFO, Hester V (2004). Occurrence of *Fusarium andiyazi* associated with sorghum in Nigeria. Archives of Phytopathology and Plant Protection 37(3):177-181.

McDonald MC, Razavi M, Friesen TL, Brunner PC, McDonald BA (2012). Phylogenetic and population genetic analyses of *Phaeosphaeria nodorum* and its close relatives indicate cryptic species and an origin in the fertile crescent. Fungal Genetics and Biology 49(11):882-895.

Minnaar-Ontong A, Herselman L, Kriel WM, Leslie JF (2017). Morphological characterization and trichothecene genotype analysis of a Fusarium Head Blight population in South Africa. European Journal of Plant Pathology 148(2):261-269.

Moschini RC, Carranza MR, Carmona MA (2004). Meteorological-based predictions of wheat head blight epidemics in the Southern Argentinian Pampas region. Cereal Research Communications 32(1):45-52.

Moussa TAA, Al-Zahrani HS, Kadasa NMS, Ahmed SA, de Hoog GS, AlHatmi AMS (2017). Two new species of the *Fusarium fujikuroi* species complex isolated from the natural environment Antonie van Leeuwenhoek 110(6):819-832.

O'Donnell K, Ward TJ, Robert VARG, Crous PW, Geiser DM, Seogchan K (2015). DNA sequence-based identification of *Fusarium*: current status and future directions. Phytoparasitica 43(5):583-595.

Parry DW, Jenkinson P, Mc Leod L (1995). Fusarium ear blight (scab) in small grain cereals – a review. Plant Pathology 44(2):207-238.

Peakall R, Smouse PE (2006). GENALEX 6: genetic analysis in Excel. Population genetic software for teaching and research. Molecular Ecology Notes 6(1):288-295.

Pestka JJ, Smolinski AT (2005). Deoxynivalenol: Toxicology and potential effects on humans. Journal of Toxicology and Environmental Health, Part B 8(1):39-69.

Ramdial H, Latchoo RK, Hosein FN, Rampersad SN (2017). Phylogeny and haplotype analysis of fungi within the *Fusarium incarnatum-equiseti* species complex. Phytopathology 107(1):109-20.

Rivera-Vargas LI, Lugo-Noel Y, McGovern RJ, Seijo T, Davis MJ (2006). Occurrence and distribution of *Colletotrichum* spp. on mango (*Mangifera indica* L.) in Puerto Rico and Florida, USA. Plant Pathology Journal 5(2):191-98.

Saremi H, Burgess LW, Backhouse D (1999). Temperature effects on the relative abundance of *Fusarium* species in a model plant-soil ecosystem. Soil Biology and Biochemistry 31(7):941-47.

Summerell BA, Leslie JF, Liew ECY, Laurence M, Bullock S, Petrovic T, Bentley AR, Howard CG, Peterson SA, Walsh JL, Burgess LW (2011). *Fusarium* species associated with plants in Australia. Fungal Diversity 46(1):1-27.

Taye W, Ayalew A, Chala A, Dejene M (2016). Aflatoxin B1 and total fumonisin contamination and their producing fungi in fresh and stored sorghum grain in East Hararghe, Ethiopia. Food Additives and Contaminants: Part B Surveillance 9(4):237-245.

Taye W, Ayalew A, Dejene M, Chala A (2018). Fungal invasion and mycotoxin contamination of stored sorghum grain as influenced by threshing methods. International Journal of Pest Management 64(1):66-76.

Thakur RP, Mathur K (2000). Anthracnose: Compendium of sorghum diseases. In Frederiksen RA, Odvody GN (Eds.). The American Phytopathological Society, St. Paul MN. pp. 10-12.

Valente MT, Desideriob F, Infantinoa A, Vale G, Abbruscatod P, Aragona M (2017). Genetic variability of *Fusarium fujikuroi* populations associated with bakanae of rice in Italy. Plant Pathology 66(3):469-79.

Van der Lee T, Zhang H, Van Diepeningen A, Waalwijk C (2015). Biogeography of *Fusarium graminearum* species complex and chemotypes: a review. Food additives and contaminants. Part A. Chemistry, analysis, control, exposure & risk assessment 32(4):453-460.

Vigier B, Reid LM, Seifert KA, Stewart DW (1997). Distribution and prediction of *Fusarium* species associated with maize ear rot in Ontario. Canadian Journal of Plant Pathology 19(1):60-65.

Vos P, Hogers R, Bleeker M, Rijans M, Van de Lee T, Hornes M, Frijters A, Pot J, Kuiper M, Zebeau M (1995). AFLP: A new technique for DNA fingerprinting. Nucleic Acids Research 23(21):4407-4414.

Wollenweber HW, Reinking OA (1935). Die Fusarien, ihre Beschreibung, Schadwirkung und Bekämpfung. Paul Parey, Berlin, Germany.

Wu F, Groopman JD, Pestka JJ (2014). Public health impacts of foodborne mycotoxins. Annual Review of Food Science and Technology 5:351-372.

Vol. 18(14), pp. 296-306, 3 April, 2019
DOI: 10.5897/AJB2018.16740
Article Number: 9295F0F60593
ISSN: 1684-5315

http://www.academicjournals.org/AJB

ACADEMIC JOURNALS
expand your knowledge

African Journal of Biotechnology

Full Length Research Paper

Copper (II) ions adsorption by untreated and chemically modified *Tectona grandis* (Teak bark): Kinetics, equilibrium and thermodynamic studies

Chijioke John Ajaelu*, Lara Ibironke and Adedotun Bamidele Oladinni

Department of Chemistry and Industrial Chemistry, Faculty of Science Bowen University, Iwo, Osun State, Nigeria.

Received 28 December, 2018; Accepted 25 February, 2019

In this study, untreated *Tectona grandis* (UTG) and citric acid- modified *T. grandis* (CAMTG) bark powder were used for the adsorption of Cu (II) ions from aqueous solution. The UTG and CAMTG were characterized by Fourier Transform Infrared (FTIR), and scanning electron microscopy (SEM). The adsorption characteristics were carried out by determining the solution pH, initial concentration of Cu (II) ions, effect of time and temperature. Langmuir, Freundlich and Temkin isotherms were used to describe the equilibrium model with Freundlich isotherm giving the best fit. The maximum monolayer adsorption capacity for CAMTG was higher than that of UTG. Also, there was about a four-fold increase in the adsorption of Cu(II) ions by CAMTG (A_o = 87.0 mg/g) over UTG (A_o = 22.9 mg/g). The kinetic data were explained by employing the pseudo-first and pseudo-second order models. The pseudo-second order kinetic model has an outstanding suitability to the experimental data. The positive enthalpy and negative free energy are indications of the endothermic and spontaneous nature of the copper (II) ion adsorption process. CAMTG is therefore, a more viable adsorbent for the removal of Cu(II) ions from aqueous solution than UTG.

Key words: Adsorption, copper, equilibrium, kinetics, *Tectona grandis*.

INTRODUCTION

The increased rate at which heavy metals such as copper are released into the environment in the 21st century has raised serious health concerns all over the world. The rapid and dangerous increase in the level of these heavy metals in the environment is due to the nonchalant attitudes to environmental safety by some industries involved in their production. Culpable industries in this respect are those of metallurgical, galvanizing, metal finishing, electroplating, mining, power regeneration, electronic devices manufacturing and tannery (Ajaelu et al., 2017). Copper toxicity, for instance, has been implicated in health related issues, among which are hyperactivity in children, depression, migraine, extreme tiredness, anorexia, premenstrual syndrome, depression, anxiety and learning disorder. Some of the methods for separation and recovery of heavy metals are ion exchange, chemical precipitation, electrocoagulation (Akyol, 2012), evaporation and membrane processes (Wang and Chen, 2009) which are used on a large scale. However, these procedures are inadequate and

*Corresponding author. E-mail: chijioke.ajaelu@bowenuniversity.edu.ng.

uneconomical when metal ions exist in relatively low concentrations (Bhatti et al., 2007). They also generate large quantities of toxic sludge and secondary pollutants thereby requiring the use of large amount of reagents (Yadava et al., 2010). The removal of toxic heavy metals from industrial wastewaters using conventional chemical approaches like adsorption, oxidation and reduction and chemical precipitation, among others (Yadav, 2010), proved to be not cost effective. Similarly, activated carbon which has been employed to reduce the amount of heavy metal to harmless level due to its operational simplicity and reuse potential (Anupam et al., 2011) remains an expensive material (Mohanty, 2005). However, in recent years, the use of plant materials for the removal of heavy metal has become a more acceptable method because it has the ability to cause a reduction in the quantities of heavy metal even at low concentrations. Biosorbents that have been adopted for reducing to harmless level the heavy metals in the environment include *Senna alata* (Ajaelu et al., 2017), sawdust (Vaishya and Prasad, 1991), grape stalks (Villaescusa et al., 2004), carrot residue (Nasernejad et al., 2005), Ethiopian pepper (Ajaelu et al., 2011), groundnut shells (Shukla and Pai, 2005), wild herbs (Al-Senanai and Al-Fawzan, 2018), rice shell (Aydin et al., 2007) and wine making waste (Alguacil et al., 2018). Also, our preliminary investigations revealed that *T. grandis* was effectual in the reduction of cadmium ions level from waste water (Ajaelu et al. 2013). *Tectona grandis* (teak) is a member of the *Lamiaceae* family. It is a large deciduous tree that is dominant in mixed hard wood forest reaching over 30 m in height in favorable conditions (Orwa et al., 2009). The plant is readily available locally.

This study, therefore, investigated the effectiveness of *T. grandis* (UTG) as an adsorbent for reducing the amount of Cu^{2+} ions in solutions. Two forms of the plant material –untreated *T. grandis* (UTG) and citric acid modified *T. grandis* (CAMTG) were tested. Characterization of UTG and CAMTG was done with SEM and FTIR. Equilibrium studies were explained by Langmuir, Freundlich and Temkin models. The kinetic studies were elucidated using Pseudo-first order and pseudo-second order models. Thermodynamic parameters such as free energy, entropy and enthalpy were also determined for the adsorptive reduction in the level of Cu^{2+} ions by UTG and CAMTG.

MATERIALS AND METHODS

All reagents used are of analytical grade. Citric acid monohydrate (CA) (Figure 1) was used in the chemical modification of the biomass. Stock solution of 1000 mgL^{-1} of Cu^{2+} from $Cu(NO_3)_2$ salt was prepared. Solutions with concentrations ranging from 20 to 100 mgL^{-1} of Cu^{2+} ions were prepared by appropriate dilution of the stock solution immediately prior to their use. The *T. grandis* biomass was obtained from a wetland situated at Iwo, Nigeria (7° 38" 01' N, 4° 11" 01' E). After harvest, the biomass was washed several times with deionized water to remove the dust particles, and then dried in an oven at 373K for 24 h. The dried biomass was crushed by a high speed electric grinder. The particles were sieved with a 500-µm mesh size and stored in a plastic bag.

Citric acid modification

The chemical modification of *T. grandis* was similar to that already described by Vaughan et al., (2001) with little modifications. 0.2 M CA was added to UTG in the ratio of 12:1 (CA: UTG, w/v) and stirred for 45 min. The oven at 50°C was used to dry the UTG/acid mixture for 2 h. This was followed by increasing the temperature of the oven to 120°C to ensure thermochemical reaction of the mixture. The dry mixture was then cooled at room temperature, after which 0.1 M NaOH was added and agitated for 1 h to neutralize any residual acid present. The CA modified *T. grandis* (CAMTG) was then washed severely with de-ionized water to remove the residual alkali. The wet CAMTG was dried in an oven at 105°C until constant weight and stored in a stoppered plastic tube.

Instrumental characterization of UTG and CAMTG

Fourier Transform Infrared Spectrophotometer, Agilent Technologies Cary 630FTIR spectrometer, was used for functional group determinations on the surface of UTG and CAMTG. A sample press, which is a portion of the ATR interface, was employed to make certain that the UTG and CAMTG were in good contact with the surface of the sensor. A region of 4,000–650 cm^{-1} at 4 cm^{-1} resolution were employed to collect the data. The surface morphologies of UTG and CAMTG were determined with scanning electron microscope (Zeiss Auriga HRSEM).

Adsorption of Safranin O

Equilibrium adsorption was determined as previously described (Ajaelu et al., 2017). In brief, batch adsorption experiments were carried out by contacting 0.5 g of CAMTG (and UTG) with 20 mL of copper solution pH in a 250-mL beaker. The samples in the beakers were then agitated on an electric shaker at 298 K with a speed of 250 rpm until equilibrium was attained. Thereafter, the mixture was filtered and the concentrations of the residual Safranin O were determined using atomic absorption spectrophotometer (PG 990, PG Instruments, Britain). The amount of Cu^{2+} adsorbed, q_e (mg/g) (Equation 1) and the corresponding removal percentage (%) (Equation 2) can be calculated by the following equations:

$$q_e = \frac{(C_o - C_e)V}{w} \quad (1)$$

$$\% \text{ sorption capacity} = \frac{(C_o - C_e)}{C_o} x100 \quad (2)$$

Where C_o (mg/L) and Ce (mg/L) are the initial concentration of Cu^{2+} and the equilibrium concentration of Cu^{2+} in solution respectively; also, V (L) and w(g) are the volume of the Cu^{2+} and weight of either UTG or CAMTG respectively.

The effect of pH was determined from pH 2 to 8 by agitating 0.2 g of CAMTG/ UTG with 20 mL of 20 mg/L solution of Safranin O dye at 298K. The reduction in the concentration of Safranin O was evaluated.

Adsorption kinetic experiments were carried out by shaking 0.3 g each of adsorbent with 120 mL of 20 - 80 mg/L Cu^{2+} solutions at pH 7 and the residual concentration was obtained. The amount of Cu^{2+}

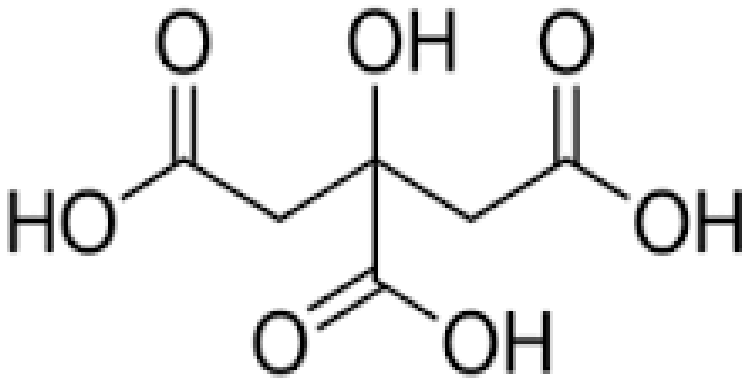

Figure 1. Structure of citric acid.

adsorbed q_t (mg/g) was obtained by the following equation:

$$q_t = \frac{C_o - C_t}{m} V \quad (3)$$

Where C_t (mg/L) depicts the amount of Cu (II) ions adsorbed at time t.

Adsorption thermodynamic experiments were carried out by agitating 20 mL of the Cu^{2+} solutions of varying concentrations (20-100 mg/L) with 0.1 g of CAMTG/UTG at varying temperatures (303, 308, 313 and 318K).

Theory

Adsorption isotherm

Langmuir, Freundlich and Temkin isotherm models were employed to illustrate the observed experimental adsorption equilibrium data. The models are stated below:

(i) The Langmuir isotherm model: For monolayer adsorption, this has gained wide application to heavy metal sorption process. The linear equation for Langmuir isotherm is

$$\frac{C_e}{q_e} = \frac{1}{A_o b} + \frac{C_e}{A_o} \quad (4)$$

Where A_o is the Langmuir maximum uptake capacity (mg/g) and b is the Langmuir constant associated with the affinity of the binding site and the energy of adsorption in $Lmol^{-1}$, q_e, is the uptake capacity at equilibrium (mg/g) and C_e is the equilibrium concentration of Cu^{2+} ions (mg/L) in solution.

A dimensionless equilibrium parameter, E_L, is a necessary characteristic of Langmuir equation and is expressed as

$$E_L = \frac{1}{(1 + aC_o)} \quad (5)$$

Where a is the Langmuir equilibrium constant in $Lmol^{-1}$ and C_o is the initial metal concentration in (mg/L).

(ii) The Freundlich isotherm model: The Freundlich equation is an empirical equation applied to explain the heterogeneous systems and is depicted as

$$\log q_e = \log g_F + \frac{1}{p} \log C_e \quad (6)$$

Where g_F (Lg^{-1}) is associated with the adsorption capacity of the adsorbent while p is a Freundlich dimensionless isotherm constant related to the heterogeneity of the surface of the adsorbent.

(iii) The Temkin Isotherm Model: Temkin isotherm (Temkin, 1941) has the assumption that the adsorption heat of the molecules will experience a linear decrease rather than a logarithmic decrease with coverage. Temkin equation is also associated with the uniform distribution of binding energy (Foo and Hameed, 2010). The linear form of the equation is given by

$$q_e = \frac{RT}{B} \ln A + \frac{RT}{B} \ln C_e \quad (7)$$

Where A is Temkin model binding equilibrium constant Lg^{-1}, and B is Temkin equilibrium constant which corresponds to the differences in adsorption energy ($kJmol^{-1}$).

The Temkin model works on the assumption that the adsorption heat of the molecules in the layer linearly decreases with coverage owing to the interaction of the adsorbent with the adsorbate, and that the uniform distribution of the binding energies describes the adsorption.

Kinetics of adsorption

UTG and CAMTG adsorption of Cu^{2+} were explained by pseudo first - order and pseudo-second order kinetic models. The linearized kinetic equation is depicted by

$$\log(q_e - q_t) = \log q_e - \frac{k_1}{2.303} t \quad (8)$$

where, k_1(min^{-1}) is the pseudo-first order rate constant for Cu^{2+} adsorption on CAMTG and UTG.

The pseudo-second order kinetic equation is

$$\frac{t}{q_t} = \frac{1}{k_2 q_e^{\,2}} + \frac{1}{q_t} t \quad (9)$$

Where k_2 (gmg $^{-1}$min $^{-1}$) is the pseudo-second order rate constant for Cu^{2+} adsorption on both CAMTG and UTG. $\frac{t}{q_t}$ min mg g $^{-1}$) is plotted against t (min) where the slope is $\frac{1}{q_t}$ (g mg $^{-1}$) and the intercept is $\frac{1}{k_2 q_e^{\,2}}$ (g min mg $^{-1}$).

The kinetic models were considered acceptable through the sum of error squares (SSE) (Ng et al., 2012), the hybrid fractional error function (HYBRID) (Kumar et al., 2008) and the Marquardt's percent standard deviation (MPSD) error function (Marquartt, 1963; Ajaelu et al., 2017). The error functions are

$$SSE = \sum_{i=0}^{Z} \left(q_{e,\exp} - q_{e,cal}\right)_i^2 \quad (10)$$

$$MPSD = 100\left(\sqrt{\frac{1}{z-j}\sum_{i=1}^{z}\left(\frac{q_{e,\exp} - q_{e,cal}}{q_{e,\exp}}\right)^2}\right)_i \quad (11)$$

$$HYBRID = \frac{100}{z-j}\sum_{i=j}^{z}\left[\frac{\left(q_{e,\exp} - q_{e,cal}\right)^2}{q_{e,\exp}}\right]_i \quad (12)$$

The kinetic fit is better when the error is low.

RESULTS AND DISCUSSION

Characterization of UTG and CAMTG

The textures of the external surfaces and morphology of UTG and CAMTG were observed by SEM as reflected in Figures 2a and 2b respectively. The UTG surface was irregular in shape and has some pores. After modification, a noticeable change was observed in the structure of CAMTG. It has broken surfaces with pores. UTG and CAMTG FTIR spectra are reflected in Figures 3a and b. The absorption at 3278 cm $^{-1}$ for UTG corresponds to OH which was shifted to 3338.7 cm $^{-1}$ in CAMTG after the addition of Cu^{2+} ion (Patel et al., 2007). The bands at 2920.4 cm^{-1} for UTG and 2818.6 cm^{-1} for CAMTG were associated with the presence of asymmetric -CH_2 and symmetric vibration of CH_2 group respectively. The bands at 1720.2 cm^{-1} for UTG and 1733.2 cm^{-1} for CAMTG represents C=O vibration of carboxylic acid. UTG shows an absorption band at 1620.1 cm^{-1} identified as N-H bend of amine (-NH_2). This was shifted to 1541.3 cm^{-1} in CAMTG after the sorption of copper (II) ion. The OH-bend of carboxylic acid on CAMTG was identified at 1438.8 cm^{-1}. The –CH_3 bend of alkane of CAMTG was located at 1369.8 cm^{-1}. The C-O stretching vibration of COOH of UTG was identified at 1309.8 cm^{-1} which was shifted to 1317.6 cm^{-1} after the sorption of copper (II) ion in CAMTG. The peak at 1238 cm^{-1} for UTG is characteristic of a C-O stretch of carboxylic acid and was shifted to 1241.2 cm^{-1} in CAMTG. The peaks at 1181.8 and 1026 cm^{-1} for UTG were assigned to the C-F stretch of alkyl halide; but were shifted to 1157.3 and 1030.6 cm^{-1} respectively, in CAMTG.

The specific surface area Q of UTG and CAMTG were calculated from the value of A_o with Q obtained as follows:

$$Q = \frac{N_A X A_o}{M} \quad (13)$$

Where N_A is the Avogadro's number, X and M are the cross-sectional area in m^2/g and the molar mass in g of the adsorbate respectively (Ali et al., 2013). The calculation of specific surface area is based on the A_o value, the atomic mass of copper, 63.5 g, and its cross-sectional area of 1.58 $Å^2$ (the radius of Cu^{2+} ions for close packed monolayer is 0.71 Å). The specific surface area of UTG for Cu^{2+} removal was 5.42 m^2/g while that of CAMTG was 20.6 m^2/g. Thus, CAMTG has wider surface area as compared to UTG which was responsible for its effectiveness in removing more Cu^{2+} ions from solution.

Effect of pH

The solution pH has impactful effect on the adsorption of Cu^{2+} on CAMTG than on UTG. From the experimental results reflected in the graph in Figure 4, it was observed that for CAMTG, there was a significant increase in adsorption from pH 2 to 7, a sharp increase from pH 6 - 7 and then a decrease. Adsorption of Cu^{2+} ions by CAMTG was better at slightly acidic to neutral pH condition than for basic environment. This is because as the pH increases from acidic to neutral pH the number of negatively charged sites increases, and adsorption of Cu on CAMTG consequently increased. These may also be due to the chemical reaction and strong electrostatic interaction of the surface of CAMTG as well as Cu^{2+} ions in solution.

UTG increased slightly with pH due to weak surface - Cu (II) ions electrostatic interaction. Thus, pH had more profound effect on CAMTG than on UTG. Similar results were obtained by some researchers (Hameed and El-Khaiary, 2008; Adebowale et al., 2014). Moreover, at lower acidic pHs the charges on the surfaces of UTG and CAMTG are positive due to the next protonation reactions of the hydroxylic sites (1):

$$\approx ZOH + H^+ \longrightarrow \approx ZOH_2^+$$

As the pH increases, the adsorbent acidic sites were

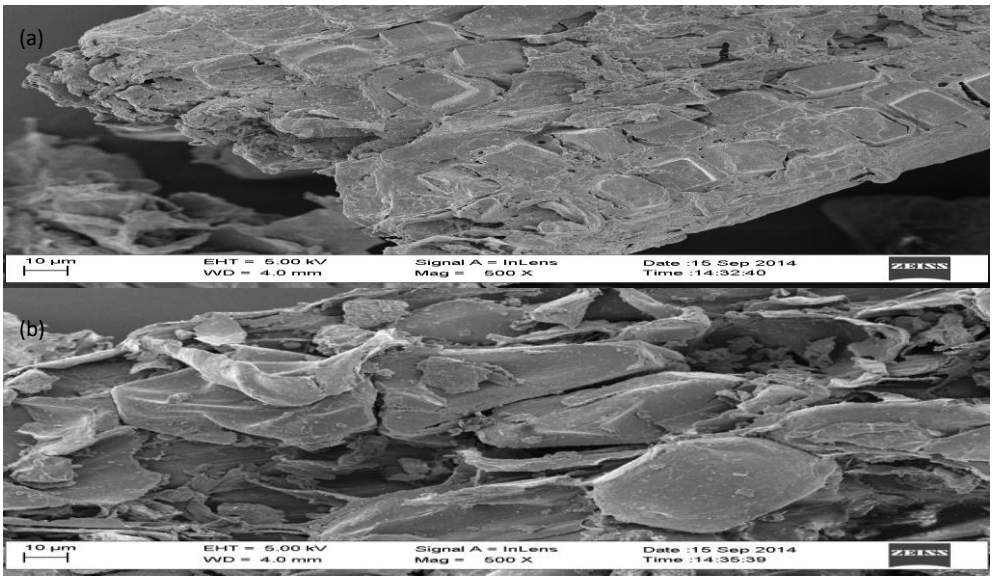

Figure 2. SEM micrograph of (a) UTG (b) CAMTG.

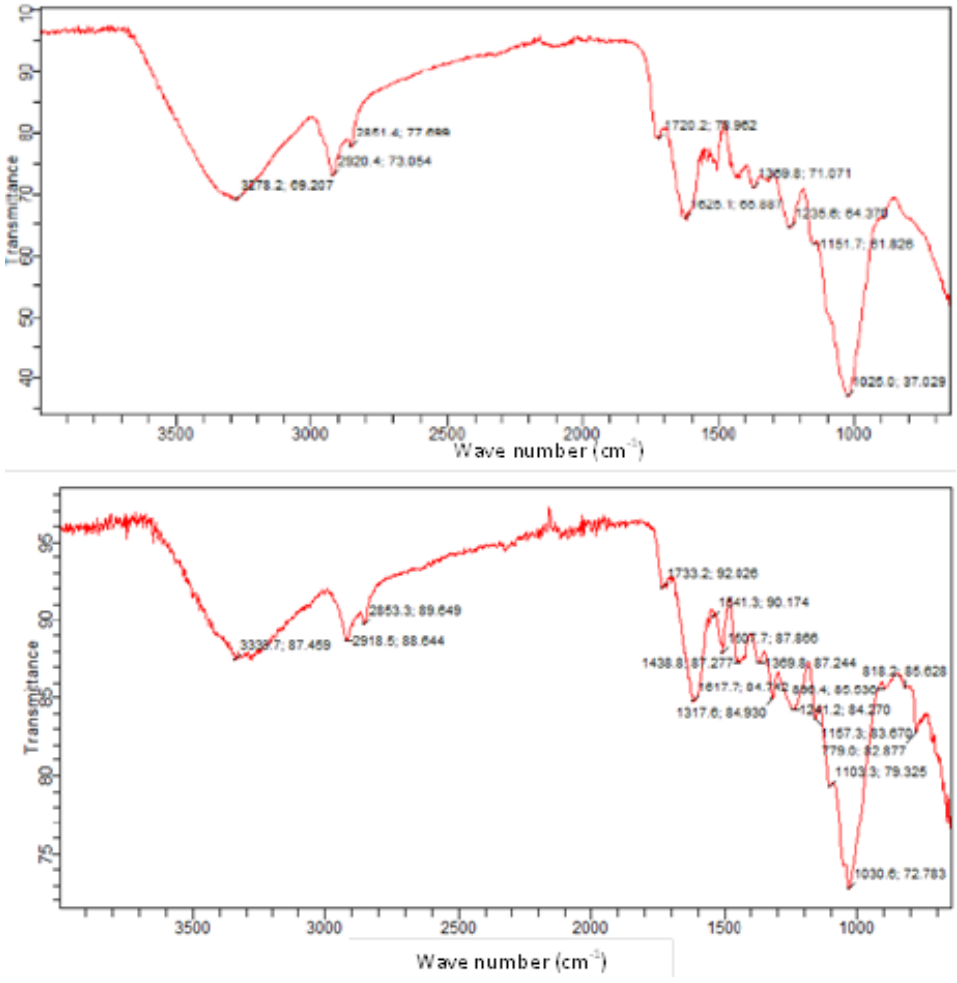

Figure 3. The spectra of FTIR for (a) UTG and (b) CAMTG.

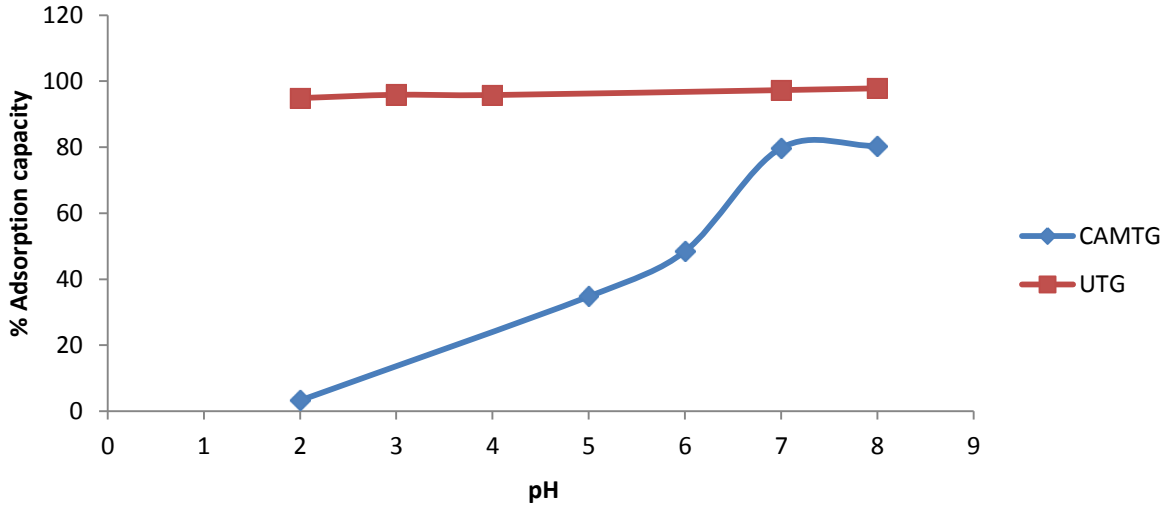

Figure 4. pH effect on the removal of copper by UTG and CAMTG.

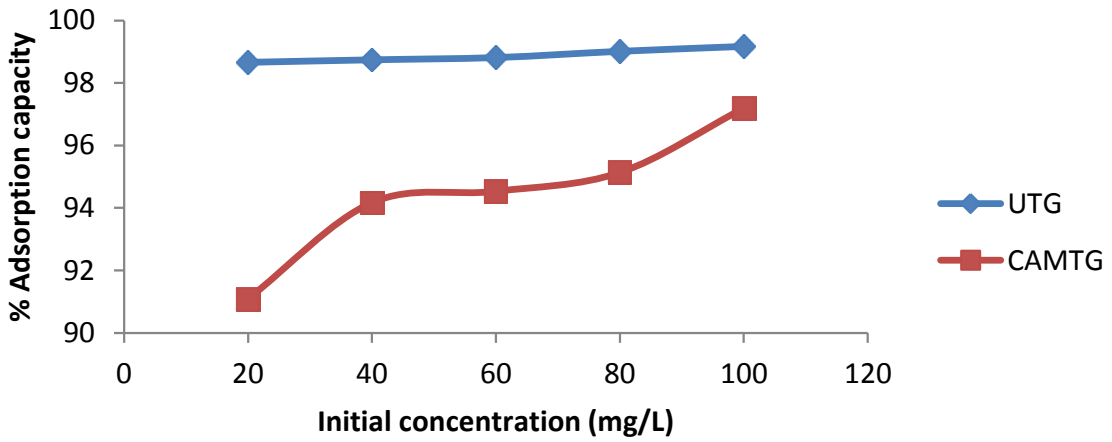

Figure 5. Initial metal concentration effect on the removal of copper from UTG and CAMTG.

deprotonated owing to the surface that were negatively charged:

$$\approx ZOH \longrightarrow ZO^{-} + H^{+}$$

The surfaces of UTG and CAMTG are represented by ≈Z. Vasconcelos et al., (2008) and Tong et al. (2011) got identical results.

Effect of initial metal concentration

The initial concentration of the metal affects the uptake capacity of CAMTG and UTG to adsorb Cu^{2+} ions as shown in Figure 5. The sorption capacity of CAMTG for Cu^{2+} ions rose sharply with initial Cu^{2+} concentration from 20 to 40 mg/L and then increased gradually from 40 to 80 mg/L. UTG sorption capacity increased slightly with initial Cu^{2+} concentrations from 20 to 100 mg/L.

Adsorption isotherm

The parameters of the adsorption isotherms are reflected in Table 1. Experimental equilibrium results show that Freundlich isotherms (Figure 7) for both UTG and CAMTG (UTG, R^2 = 0.97 and CAMTG, R^2 = 0.99) fitted best when compared to that of Langmuir in Figure 6 (UTG, R^2 = 0.91 and CAMTG, R^2 = 0.91) and Temkin in Figure 8 (UTG, R^2 = 0.91 and CAMTG, R^2 = 0.88).

Freundlich isotherm fitted better for CAMTG (R^2 = 0.99) than for UTG (R^2 = 0.97). In addition, the values of n are greater than unity for both UTG and CAMTG which indicate that the values of n are greater than unity for

Table 1. Equilibrium results for Cu^{2+} ions adsorption on UTG and CAMTG at 303K.

Isotherm models	Parameter	
	UTG	CAMTG
Freundlich	$g_F = 8.34$ p = 2.22 R^2 = 0.97	$g_F = 1.69$ p = 1.33 R^2 = 0.99
Langmuir	Ao = 22.9 mg/g b = 0.53 L/mg R^2 = 0.91 RL = 0.018	Ao = 87.0 mg/g b = 0.01 L/mg R^2 = 0.91 RL = 0.42
Temkin	A = 1.68 B = 23.1 R^2 = 0.9	A = 2.70 B = 297.4 R^2 = 0.88

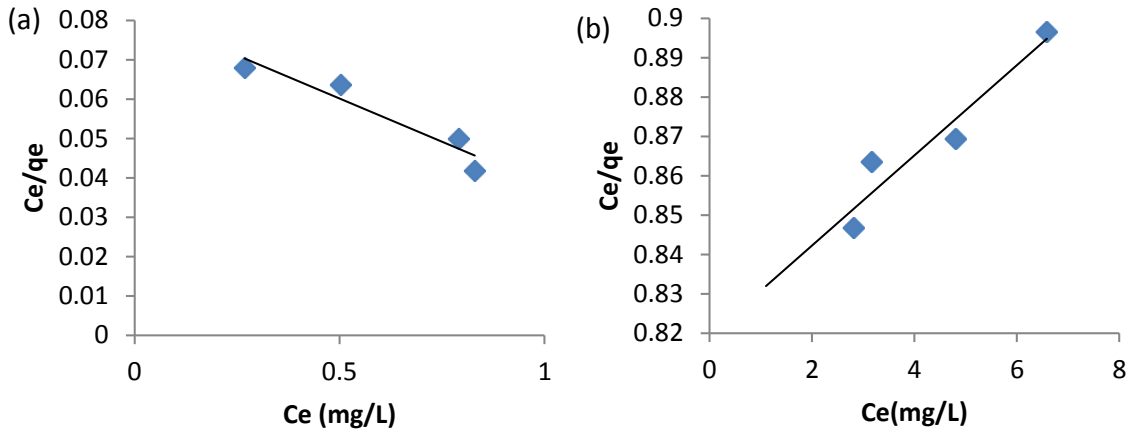

Figure 6. The plot of Ce/qe vs Ce showing the Langmuir isotherm for the removal of Cu^{2+} by (a) UTG and (b) CAMTG.

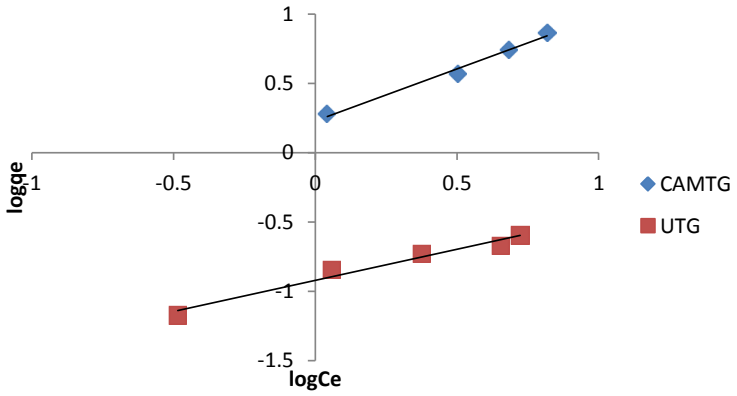

Figure 7. Freundlich isotherm for the removal of Cu^{2+} ions by UTG and CAMTG.

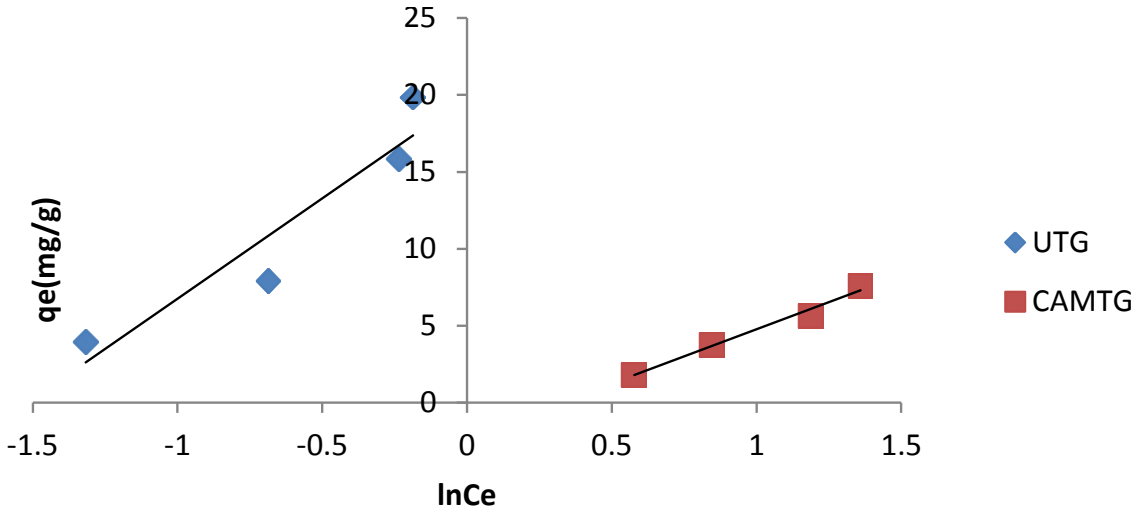

Figure 8. Temkin isotherm for the removal of Cu (II) ions by UTG and CAMTG.

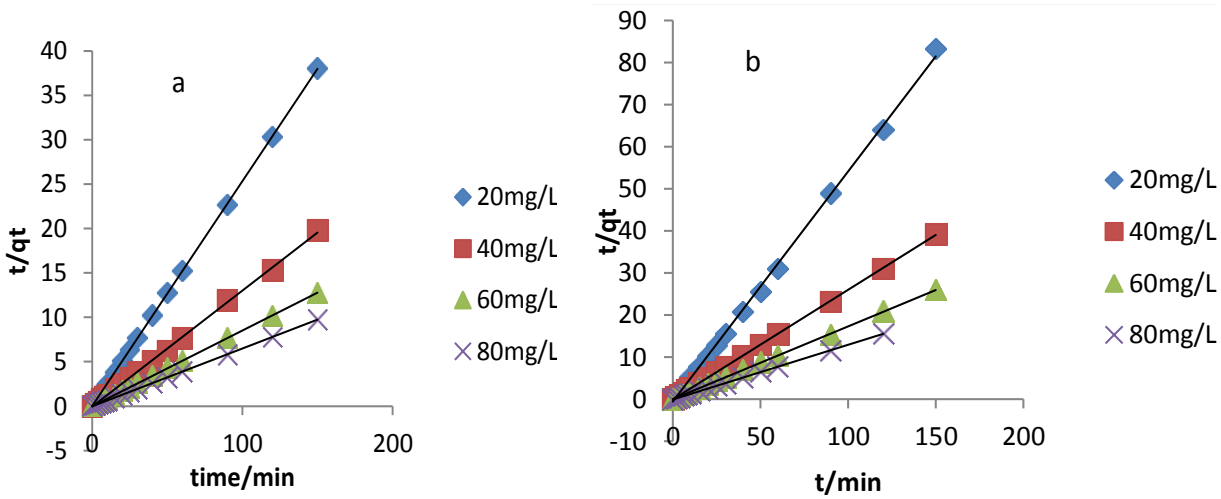

Figure 9. Pseudo second order kinetics for the uptake capacity of (a) UTG and (b) CAMTG on Cu^{2+} ions.

both UTG and CAMTG which implied the favorability and intensity of adsorption of Cu^{2+} ions on the surfaces of both UTG and CAMTG. The Langmuir maximum adsorption capacity of CAMTG (87.0 mg/g) is higher than that of UTG (22.9 mg/g). This is an increase of about four-fold in Cu^{2+} ions adsorption by CAMTG over UTG, implying that the citric acid modification of the untreated *T. grandis* increased the number of active sites available for adsorption, and consequently enhance the electrostatic interaction between Cu^{2+} ions and CAMTG. Langmuir isotherm efficiency can also be buttressed by determining whether the adsorption is favourable or not, using the separation factor, R_L, also known as the dimensionless equilibrium parameter. Both UTG (R_L = 0.02) and CAMTG (R_L = 0.42) have R_L<1. Thus the sorption of Cu^{2+} ions on both UTG and CAMTG is favourable.

Effect of adsorption kinetics

The kinetic plots of pseudo-second order reaction is presented in Figure 9. The pseudo-first order kinetic plot gave a poor fit and, therefore, cannot be used to explain the sorption of Cu^{2+} ions on both UTG and CAMTG. The kinetic results are presented in Table 2. The calculated values of sorption capacity using Equation 9 which is reflected in Table 2 for a pseudo-second order kinetic gave strong agreement with the experimental values (q_{exp}), and excellent results for the correlation coefficients were obtained. There was increase in the values of q_{calc} as the concentration rose from 20 to 80 mg/L for both

Table 2. Sorption kinetic parameters for the adsorption of Cu^{2+} ions on UTG and CAMTG.

	UTG	Pseudo first order			CAMTG	Pseudo first order		
C_o(mg/L)	**20**	**40**	**60**	**80**	**20**	**40**	**60**	**80**
$q_{e(exp)}$	3.95	7.9	11.9	15.8	1.82	3.77	5.67	7.22
k_1(min $^{-1}$)	0.014	0.08	0.01	0.05	0.015	0.015	0.01	5x10 $^{-4}$
$q_{e(cal)}$	4.85	5.17	2.93	4.21	4.85	4.85	3.8	3.93
SSE	0.64	1.93	6.31	8.23	2.14	0.76	1.32	2.33
HYBRID	6.82	31.4	223.9	284.8	167.3	10.3	20.6	30
MSPD	13.2	20	43.5	42.4	95.8	16.6	19.1	26.3
	UTG	**Pseudo Second order**			**CAMTG**	**Pseudo Second order**		
$q_{e(cal)}$	3.95	7.65	11.8	15.4	1.03	3.84	5.79	7.72
k_2(gmg $^{-1}$min^{-1})	2.64	1.02	6.97	11.8	0.53	7.57	3.37	2.85
R^2	1	0.99	0.99	0.95	0.99	0.99	1	0.99
SSE	4.0X10^{-3}	0.18	0.08	0.31	1x10^{-3}	0.05	0.08	0.36
HYBRID	3.0X10^{-4}	0.26	0.32	0.4	7x10^{-4}	0.05	0.08	0.05
MPSD	0.09	1.81	0.52	1.58	0.2	1.13	1.17	3.96

UTG and CAMTG. Thus, pseudo-second order kinetic model was preferred in describing the Cu^{2+} sorption onto UTG and CAMTG.

Moreover, only the pseudo-second order model, in which the metal binding capacity is assumed proportional to the number of active sites occupying the sorbents (UTG and CAMTG), gave a good representation of the sorption rate (Ajaelu et al., 2017; Ferreira et al., 2011).

Error Equations 10, 11 and 12 were used to describe the appropriateness of the kinetic models for the sorption of Cu^{2+} ions on UTG and CAMTG. The model fits well if the error value is minimized. Table 2 showed that the SSE, HYBRID and MPSD values obtained for UTG and CAMTG were lower for pseudo-second order kinetic than for pseudo-first order kinetic models. This, of a certainty, showed that pseudo second order kinetic model described better the sorption of Cu^{2+} ions on UTG and CAMTG.

Thermodynamic effect

To study the effect of temperature, experiments were carried out at different temperatures of 303, 308, 313 and 328K and different concentrations of 20, 40, 60 and 80 mg/L, respectively. It was observed that temperature has a greater effect on CAMTG than on UTG. Moreover, at a particular temperature, concentration increase enhances the quantity of Cu^{2+} ions adsorbed on the surfaces of both UTG and CAMTG.

The thermodynamic parameters were obtained from the following equations:

$$\ln K_d = \frac{q_e}{C_e} \quad (14)$$

$$\Delta G = - RT\ln K_d \quad (15)$$

$$\ln K_d = -\frac{\Delta G}{RT} = \frac{\Delta S}{R} - \frac{\Delta H}{RT} \quad (16)$$

Where K_d, is the ratio of Cu^{2+} ions adsorbed at equilibrium to that left in the solution at equilibrium. R is the universal gas constant in J mol $^{-1}$K $^{-1}$, T is the absolute temperature in K, Δ*G* (kJmol $^{-1}$) is the Gibbs free energy of adsorption, Δ*H* is the enthalpy change (kJmol $^{-1}$) while Δ*S* (Jmol $^{-1}$K $^{-1}$) is the entropy change. The various values of Δ*H* and Δ*S* were obtained from the slopes and intercepts of the plot of $\ln K_d$ against 1/T (as presented in Figures 10a and b) at different Cu^{2+} ions concentrations of 20 to 80 mg/L and the results are listed in Table 3. It is evident from Table 3 that the sorption of Cu^{2+} ions on both UTG and CAMTG are endothermic and spontaneous as reflected in the positive values of Δ*H* and the negative values of Δ*G*. Thus, high temperatures enhanced the dehydration procedure and therefore, the adsorption process. Similar results were obtained by Gupta and Sharma (2002), and Chen and Wang (2006). The enthalpy changes necessary to accomplish the adsorption process was lower for CAMTG (9.23-25.6 kJ mol^{-1}) than for UTG (3.62-34.5 kJ mol^{-1}). This may be due to the existence of additional available pores for sorption in CAMTG than in UTG. The values of ΔG for both UTG and CAMTG are negative, which are indications that the sorption processes were spontaneous. Δ*S* was also an indication of the good affinity of adsorbent for adsorbate and increased randomness during the adsorption process (Ajaelu et al., 2017). In addition, the positive value of the entropy ΔS indicated that the increasing entropy, as a result of solvent desorption, was higher than reduction of

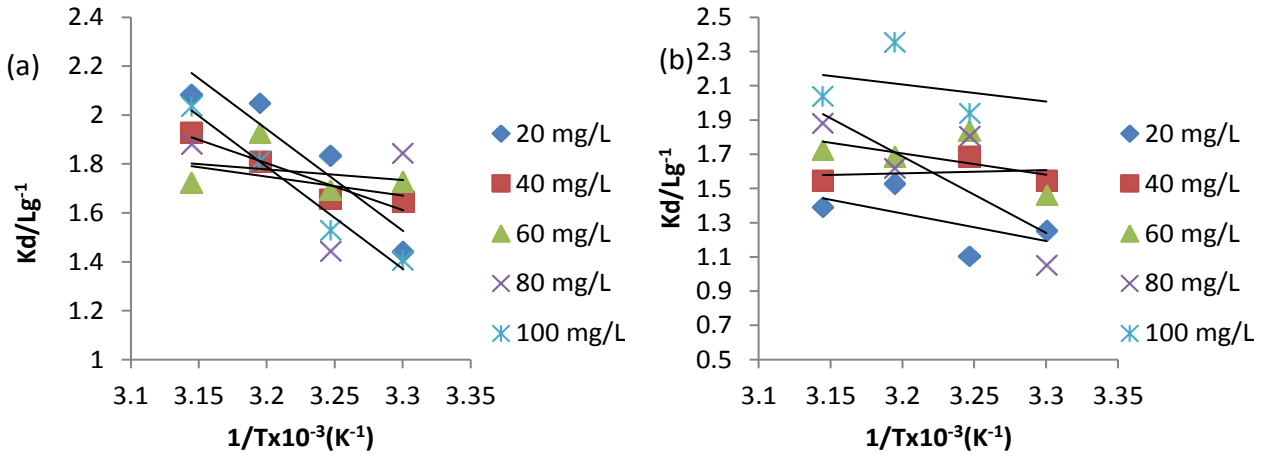

Figure 10. The plot of lnK against T^{-1}/K^{-1} for the sorption of Cu^{2+} ions onto UTG and CAMTG.

Table 3. Thermodynamic parameters for the uptake of Cu^{2+} ions by UTG and CAMTG.

Adsorbent	Metal Conc. (mg/L)	ΔH (kJ/mol)	ΔS (J/molK)	ΔG (kJ/mol) 303K	308K	313K	318K
UTG	20	34.5	126.6	- 3.63	- 4.7	- 5.33	- 5.51
CAMTG	20	21.8	78.4	- 3.16	- 2.83	- 3.98	- 3.68

Table 4. Adsorption capacities of various adsorbents.

Adsorbent	Adsorption capacity (mg/g)	Temp. (K)	References
Capsicum annuum	28.6	323	Ozcan et al., (2005)
Irish peat moss	17.6	298	Gupta et al., (2009)
Wheat shell	17.4	338	Aydin et al., (2008)
Tamarindus indica seed powder	83	303	Chowdhury and Saha (2008)
Spent grain	10.5	-	Lu and Gib, (2008)
Garlic - treated *Canna indica*	27.9	-	Mahamadi and Chapeyama (2011)
UTG	22.9	303	This study
CAMTG	87	303	This study

entropy caused by solute adsorption ((Vaishya and Prasad, 1991).

Table 4 shows the comparison of adsorption capacities for various adsorbents at different temperatures. It is obvious that CAMTG adsorbed best among all the other adsorbents.

Conclusion

This study examined the interaction of Cu (II) ion with the surface of untreated (UTG) and citric acid modified *T. grandis* (CAMTG) leaves powder. The effect of pH on the adsorption of Cu (II) by CAMTG was more pronounced than that of UTG. The surface area of CAMTG was about four-fold that of UTG. Consequently, the ratio of maximum monolayer adsorption of CAMTG to UTG is 4:1. Strong electrostatic interaction between Cu (II) ions and the adsorbents enabled pseudo-second order kinetic model to appropriately describe the adsorption of Cu (II) ions on both UTG and CAMTG at different concentrations of Cu (II) ions. Thermodynamic parameters determined showed that the metal adsorption process was endothermic and spontaneous. Citric acid modified *T. grandis* can be deployed to effectively reduce the amount of Cu (II) ions from aqueous solution.

CONFLICT OF INTERESTS

The authors have not declared any conflict of interests.

REFERENCES

Adebowale KO, Olu-Owolabi BI, Chigbundu EC (2014). Removal of Safranin O from aqueous solution by adsorption onto Kaolinite clay. Journal of Encapsulation and Adsorption Science 4:89-104.

Ajaelu CJ (2013). Kinetics and equilibrium studies of cadmium (II) ions adsorption onto *Tectona grandis* (Teak Plant) seed. Proceedings of the 36th Annual International Conference of the Chemical Society of Nigeria 1:461-473.

Ajaelu CJ, Dawodu MO, Faboro EO, Ayanda OS (2017). Copper Biosorption by Untreated and Citric Acid Modified *Senna alata* Leaf Biomass in a Batch System: Kinetics, Equilibrium and Thermodynamics Studies. Physical Chemistry 7(2):31-41.

Ajaelu CJ, Ikotun AA, Olutona OO, Ibironke OL (2011). Biosorption of aqueous solution of lead on *Xylopia aethiopica*. Journal of Applied Science in Environmental. Sanitation 6(3):269-277.

Akyol A (2012). Treatment of paint manufacturing wastewater by electrocoagulation. Desalination 285:91-99.

Alguacil FJ, Alcaraz L, Garcia-Diaz I, Lopez FO (2018). Removal of Pb^{2+} from waste water via adsorption unto an activated carbon produced from wine making waste. Metal 697(8):1-15.

Al-senanai GM, Al-Fawzan FF (2018). Adsorption study of heavy metal ions from aqueous solution of nanoparticles of wild herbs. The Egyptian Journal of Aquatic Research 44(3):187-194

Ali SZ, Atha M, Farooq U, Salman M (2013). Insight into Equilibrium and Kinetics of the Binding of Cadmium Ions on Radiation - Modified Straw from *Oryza sativa*. Journal of Applied Chemistry pp. 1-12. https://www.hindawi.com/journals/jac/2013/417180/

Anupam K, Dutta S, Bhattacharjee C, Datta S (2011). Adsorptive removal of chromium (IV) from aqueous solution over powdered activated carbon: Optimization through response surface methodology. Chemical. Engineering Journal 173:135-143.

Aydin H, Bulut Y, Yerlikaya C (2008). Removal of Cu (II) from aqueous solution by adsorption onto low-cost adsorbents. Journal of Environmental Management 87(1):37-45.

Bhatti HN, Mumtaz B, Hanif MA, Nadeem R (2007). Removal of Zn(II) ions from aqueous solution using *Moringa oleifera* Lam. (horseradish tree) biomass. Process Biochemistry 42(4):547-553.

Chen CL, Wang XK (2006). Adsorption of Ni(II) from aqueous solution using oxidized multiwall carbon nanotubes Industrial. Engineering Chemical Research 45:9144-9149.

Chowdhury S, Saha PD (2011). Biosorption, kinetics, thermodynamics and isosteric heat of absorption of Cu(II) unto *Tamarindus indica* seed powder. Colloids and Surface B: Biosurfaces 88:697-705.

Ferreira LS, Rodrigue, MS, de Carvalho JCM, Lodi A, Finocchio E, Perego P, Converti P (2011). Adsorption of Ni^{2+}, Zn^{2+} and Pb^{2+} onto dry biomass of *Arthrospira (Spirulina) platensis* and *Chlorella vulgaris*. I. Single metal systems. Chemical Engineering Journal 173:326-333.

Foo KY, Hameed BH (2010). Insight into the modeling of adsorption isotherm systems. Chemical Engineering Journal 156(1):2-10.

Gupta VK, Sharma S (2002). Removal of cadmium and zinc from aqueous solution of red mud. Environmental Science Technology 36(16):3612-17

Gupta BN, Curran M, Hasan S, Ghosh TK (2009). Adsorption characteristics of Cu and Ni on Irish peat moss. Journal of Environmental Management 90(2):954-960.

Hameed BH, El-Khaiary MI (2008). Sorption kinetics and isotherm studies of a cationic dye using agricultural waste: Broad bean peels. Journal of Hazardous Materials 154(1-3):639-648.

Kumar KV, Porkodi K, Rocha F (2008). Isotherms and thermodynamics by linear and non-linear regression analysis for the sorption of methylene blue onto activated carbon: comparisons of various error functions. Journal of Hazardous Material 151(2-3):794-804.

Lu S, Gibb SW (2008). Copper removal from waste water using spent-grain as biosorbent. Bioresource Technology 99(6):1509-1517.

Mahamadi C, Chapeyama R (2011). Divalent metal ion removal form aqueous solution by acid-treated and garlic-treated *Canna indica* roots. Journal of Applied Science and Environmental Management 15(1):97-103.

Marquartt DW (1963). An algorithm for least square estimation of non-linear parameters. Journal of Social, Industrial and Applied Mathematics 11(2):431-441.

Mohanty K (2005). Removal of Chromium (VI) from dilute aqueous solutions by activated carbon developed from *Terminalia arjuna* nuts activated with zinc chloride. Chemical Engineering Journal 60(11):3049-3059.

Nasernejad B, Zadeh TE, Pour BB, Bygi ME, Zamani A (2005). Comparison for biosorption modeling of heavy metals (Cr(III), Cu(II), Zn(II)) adsorption from wastewater by carrot residues. Process Biochemistry 40(3):1319-1322.

Ng JCY, Cheung WH, Mckay G (2012). Equilibrium studies of the sorption of Cu (II) ions onto chitosan. Journal of Colloid Interface Science 255(1):64-74.

Orwa C, Mutua A, Kindt R, Jamnadass R, Anthony S (2009). Agroforestry Database: a tree reference and selection guide version 4.0. World Agroforestry Centre, Kenya. http://www.worldagroforestry.org/output/agroforestree-database

Ozcan A, Ozcan AS, Tunali S, Akar T, Kiran I (2005). Determination of the equilibrium, kinetics and thermodynamic parameters of adsorption of Cu(II) ions on seeds of *Capsicum annuum*. Journal of Hazardous Materials 124(1-3):200-208.

Patel HA, Somani RS, Bajaj HC, Jasra RV (2007). Preparation and Characterization of Phosphonium Montmorillonite with Enhanced Thermal Stability. Applied Clay Science 35(3-4):194-200.

Shukla SR, Pai, RS (2005). Adsorption of Cu(II), Ni(II) and Zn(II) on dye loaded groundnut shells and sawdus Seperation. Purification Technology 43(1):1-8.

Temkin MI (1941). Adsorption equilibrium and the kinetics of processes on nonhomogeneous surfaces and in the interaction between adsorbed molecules. Zhurnal Fizicheskoi Khimii 15:296-332.

Tong KS, Kassim MJ, Azraa A (2011). Adsorption of Cu ions from its aqueous solution by a novel biosorbent *Ncaria gambir*: Equilibrium, kinetic and thermodynamic studies. Chemical Engineering Journal 170(1)145-153.

Vaishya RC, Prasad SC (1991). Adsorption of copper(II) on sawdust. Indian Journal of Environmental Protection 11(4):284-289.

Vasconcelos HL, Camargo TP, Gong-alves NS, Neves A, Laranjeira MCM, Fa´vere VT (2008). Chitosan crosslinked with a metal complexing agent: Synthesis, characterization and copper (II) ions adsorption. Reactive & Functional Polymers 68(8):572-579.

Vaughan T, Seo CW, Marshall WE (2001). Removal of selected metal ions from aqueous solution using modified corncobs. Bioresource Technology 78(2):133-139.

Villaescusa I, Fiol N, Martinez M, Miralles N, Poch J, Serarols J (2004). Removal of copper and nickel ions from aqueous solutions by grape stalks wastes. Water Resource 38(4):992-1002.

Wang JL, Chen C (2009). Biosorbents for heavy metals removal and their future: A review. Biotechnology Advancement 27(2):195-226.

Yadava NK, Sreekrishnanc TR, Satyad S, Bishnoib NR (2010). Removal of chromium and nickel from aqueous solution in constructed wetland: Mass balance, adsorption-desorption and FTIR study. Chemical Engineering Journal 160(1):122-128.

Vol. 18(14), pp. 307-315, 3 April, 2019
DOI: 10.5897/AJB2018.16557
Article Number: 6948BBD60595
ISSN: 1684-5315

http://www.academicjournals.org/AJB

ACADEMIC JOURNALS
expand your knowledge

African Journal of Biotechnology

Full Length Research Paper

Complete genomic sequence and recombination analysis of *wheat yellow mosaic virus* isolate from Zhouzhi in China

Zong-Ying Zhang[1], Cui-Ji Zhou[1], Yun-Feng Wu[2], Da-Wei Li[1], Jia-Lin Yu[1] and Cheng-Gui Han[1*]

[1]Department of Plant Pathology and State Key Laboratory for Agrobiotechnology, China Agriculture University, 100193 Beijing, China.
[2]Department of Plant Pathology, Northwest A&F University, 712100 Yangling, China.

Received 15 June 2018; Accepted 21 November, 2018

Wheat yellow mosaic virus (WYMV) is the causal agent of wheat yellow mosaic disease in China. WYMV was detected in wheat sample collected from Zhouzhi of Shanxi province. The nearly complete genomic sequence of Zhouzhi isolate (WYMV-ZZ) was determined; it was compared with six complete sequences of WYMV isolates (five Chinese isolates and one Japanese isolate). WYMV-ZZ and the other six different WYMV isolates shared 96.6 to 97.7% and 95.1 to 98.2% nucleotide sequence identity for RNA1 and RNA2, respectively; at the amino acid level, WYMV-ZZ had 94.1 to 98.2% identity for RNA1 and 94.1 to 96.7% identity for RNA2, respectively, with the other six isolates. Phylogenetic analysis showed that the NIa-VPg region can separate the Chinese isolates from Japanese isolate. Based on the recombinant analysis, there were three possible recombination events; one event was located in RNA1 CI region of WYMV-ZZ with a RDP *P*-value of 8.526×10^{-06}. This work advanced our understanding of the WYMV molecular variation and was helpful to study the disease spread.

Key words: Sequence comparison, phylogenetic analysis, NIa-VPg, recombinant event.

INTRODUCTION

Wheat yellow mosaic virus (WYMV), is the causal agent of wheat yellow mosaic disease of wheat in China and Japan, belongs to the genus *Bymovirus* within the family Potyviridae and is a soil-borne pathogen, it is transmitted by the fungus-like organism *Polymyxa graminis* (Sawada, 1927). In China, the disease was found in Sichuan province in the 1960s (Tao et al., 1980) and spread gradually to the middle and lower valleys of the Yangtze and Huai Rivers (Li et al., 1997; Chen, 1999). Wheat yellow mosaic virus causes typical symptoms including mosaic, yellowing, dwarfing, stunting or excessive tillering, and subsequently decreasing yield. Under low-temperature conditions in the field, WYMV infects wheat. When spring comes, the infected wheat shows light green, oval- or spindle-shape spots; the temperature back to 10°C, the infected leaves show yellow mosaic symptom with the disease spots expand and emerge. Finally, WYMV causes serious damage as a result of

*Corresponding author. E-mail: hanchenggui@cau.edu.cn. Fax: +86-010-62813758.

yield losses (Wang et al., 2015).

The genome of WYMV is composed of two (+) single-stranded RNAs, RNA1 encodes for P3, pretty interesting Potyviridae ORF (PIPO), 7K, cytoplasmic inclusion protein (CI), 14K, nuclear inclusion protein a (NIa) which contains viral genome-linked protein (VPg) and C-terminal protein, nuclear inclusion protein b (NIb) and coat protein (CP); RNA2 encodes for a polyprotein that contains 28- and 72-kDa proteins (Chen et al., 1999; Clover and Henry, 1999; Yu et al., 1999).

Full-length of five Chinese WYMV isolates and one Japanese WYMV isolate have been detected including isolate that came from Huangchuan, Henan province (WYMV-HC) (Yu et al., 1999); from Yangzhou, Jiangsu province (WYMV-YZ) (Chen et al., 2000); from Ya'an, Sichuan province (WYMV-YA) (Chen et al., 2000); from Japan (WYMV-JPN) (Namba et al., 1998); from Zhumadian, Henan province (WYMV-ZMD) (Zhang et al., 2010); and from Xiaqiao, Jiangsu province (WYMV-XQ with GenBank accession numbers FJ361764 and FJ361767). In this study, WYMV was detected in wheat leaves collected from Zhouzhi, Shanxi province where WYMV has not been reported before. The complete sequence of Zhouzhi isolate (WYMV-ZZ) was cloned, sequenced and compared with the other six complete sequences. Phylogenetic and recombination analyses were performed among these seven isolates.

The analysis of virus sequence and identification of virus type are helpful for breeding wheat resistant varieties (Jin et al., 2016). Full-length of five Chinese WYMV isolates and one Japanese WYMV isolate have been retrieved from GenBank database (Table 2) including isolate that came from Huangchuan, Henan province (WYMV-HC) (Yu et al., 1999); from Yangzhou, Jiangsu province (WYMV-YZ) (Chen et al., 2000); from Ya'an, Sichuan province (WYMV-YA) (Chen et al., 2000); from Zhumadian, Henan province (WYMV-ZMD) (Zhang et al., 2010); from Xiaqiao, Jiangsu province (WYMV-XQ); and from Japan (WYMV-JPN) (Namba et al., 1998).

MATERIALS AND METHODS

Sample

Wheat sample was collected from Zhouzhi, Shanxi province of China in 2008.

Total RNA extraction, reverse transcription-polymerase chain reaction (RT-PCR) and sequencing

Total RNA from wheat leaves was extracted by LiCl precipitating method (Zhang et al., 2011). Primer VP-1M was used for reverse transcription (RT) reaction and primer pair VP-1P/VP-1M was used to amplify a 704 bp fragment which was the VPg region in RNA1; primer ut-1M was used for RT reaction and primer pair ut-1P/ut-1M was used to amplify a 880 bp fragment which was the 3-termino-UTR in RNA2 (Ohto and Sakai, 2005). The purified bands were cloned into pMD18-T vector and 2-3 clones were sequenced by companies (Introvigen and BiMad). The sequence fragments were combined together by DNAMAN 7.0.

Western blotting

The wheat leaves were grinded by liquid nitrogen, added 2×SDS protein buffer, blended and incubated at 100°C for 5 min, then put the samples on the ice for 5 min, and centrifuged 12,000 rpm for 10 min; the supernatant was carried onto the SDS polyacrylamide gel electrophoresis. After electrophoresis, the sample was transferred to Hybond-C membrane, and the membrane was incubated with TBST buffer (20 mM Tris, 137 mM NaCl, 0.3% Tween20, pH 7.6) containing 5% skimmed milk powder for 2 h at 37°C and added antiserum of WYMV-CP which was prepared by Yan-hong Han storing in my lab to incubate for 1 h at 37°C. Blot was rinsed by TBST for 3 times and incubated for 1 h with anti-goat IgG diluted 1:10,000. After washing in TBST, blot was visualized by NBT and BCIP (Han et al., 2002).

Phylogenetic analysis

To better understand the relationship of WYMV-ZZ and other six WYMV isolates, the full-length sequence alignments and phylogenetic analysis of nucleotide and amino acid were conducted. Phylogenetic trees were constructed for by the neighbor-joining method and visualized using MEGA X (Molecular Evolutionary Genetics Analysis version X) with 1000 bootstraps replicate (https://www.megasoftware.net) (Kumar et al., 2018).

Recombination analysis

Recombination of seven WYMV isolates was constructed by RDP4.97 (Recombination Detection Program version 4.97) (Martin et al., 2015). Various recombination detection methods were used to analyze putative recombinants and recombination breakpoints, including the programs RDP, GENECONV, BOOTSCAN, MAXCHI, SISCAN and 3SEQ. The recombination events which were surveyed by at least five different methods could be received (Zhou et al., 2012).

RESULTS

Detection of WYMV-ZZ by RT-PCR and Western blotting

WYMV-ZZ was detected from wheat sample of Zhouzhi, Shanxi province using RT-PCR and Western blotting (Figure 1).

Complete genomic sequence of WYMV-ZZ and its comparison with other six isolates

The genomic RNA sequence of WYMV-ZZ was obtained from the wheat sample by amplification of four overlapping cDNA fragments for RNA1 and two overlapping cDNA fragments for RNA2 using the primer pairs WY1001F/WY11920R, WY11858F/WY13832R, WY13578F/WY15446R, WY15378F/HC511-BHR for RNA1, and WY2001F/WY22012R, WY21927F/HC511-

Table 1. Primers used for RT-PCR and determining full-length sequences.

Primer	Sequence (5′-3′)	Genomic position
WY1001F	AAA AATAAATAACACAGACCAAAACCATCAAAACG (+)	RNA1, 1-36 nt
WY11920R	TGATACAAGCCTGGATCCGTTGC (-)	RNA1, 1920-1898 nt
WY11858F	CACGCAATGGATCCAGGCTTCATA (+)	RNA1, 1858-1881 nt
WY13832R	CTGGCTCTGCGCGGTCTGATATCTT	RNA1, 3832-3808 nt
WY13578F	TATTGAAGATGACTCCAGCGATG (+)	RNA1, 3578-3600 nt
WY15446R	AACTTCCTGCTCGCTGAGATGTGC	RNA1, 5446-5423 nt
WY15378F	ACTTCCGCCGGACCAAGCTACCAG (+)	RNA1, 5378-5401 nt
WY2001F	AAAATAAAACCACCACAAACAAAAC (+)	RNA2, 1-26nt
WY22012R	CTGAATTGTTGCTGGTGAGACATCAT	RNA2, 2102-2077 nt
WY21927F	GAAATCTCCAAGAGCTTCAAGCAGTCA (+)	RNA2, 1927-1953 nt
HC511-BHR	GGATATCTGCAGGATCCAAGC (-)	universal primer
OligdT	GGATATCTGCAGGATCCAAGCTTTTTTTTTTTTTTTTT (-)	universal primer
VPg-1P	TGAAGATGACTCCAGCGATG (+)	RNA1, 3578-3587 nt
VPg-1M	GACCTGGGATAGGAGAATTC (-)	RNA1, 4281-4262 nt
ut-1P	CTTAAGAGGTGGAGCACGGA (+)	RNA2, 2736-2755 nt
ut-1M	GACGATCGACAGGTGCATTG (-)	RNA2, 3595-3576 nt

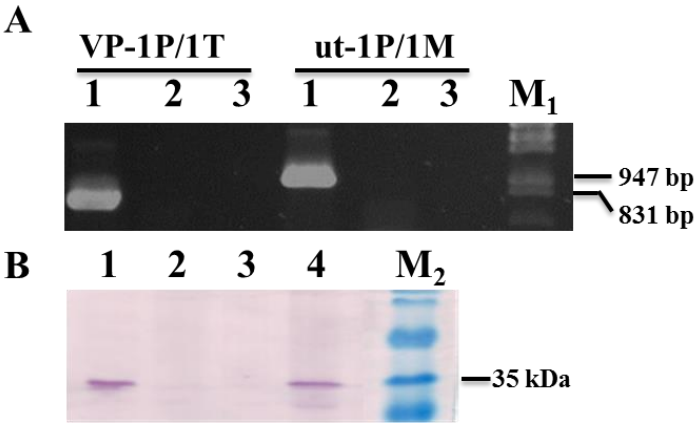

Figure 1. Result of RT-PCR (A) and western blotting (B). Lane 1: Wheat sample from Zhouzhi; Lane 2: Healthy control; Lane 3: Mock; Lane 4: Positve control; M_1: λ DNA digested by *Hin*d III and *Eco*R I; M_2: Protein marker (SM 0671, NEB).

BHR for RNA2 (Table 1). These primers were derived from the conserved region of six known isolates. A nearly complete nucleotide sequence of WYMV was determined, apart from short regions where the primers annealed at the 5'- and 3'-terminus. The full-length sequence of WYMV was submitted to GenBank with accession number FJ261765 for RNA1 and FJ361768 for RNA2 (Table 2).

Based on the full-length nucleotide comparison, WYMV-ZZ shared 96.6 to 97.7% and 95.1 to 98.2% nucleotide sequence identity for RNA1 and RNA2, respectively, with the other six isolates (WYMV-HC, WYMV-YA, WYMV-YZ, WYMV-XQ, WYMV-ZMD, WYMV-JPN). At the amino acid level, WYMV-ZZ had 94.1 to 98.2% identity for RNA1 and 94.1 to 96.7% identity for RNA2, respectively, with other six isolates; the identity for genes of RNA1 and RNA2 was >90% between WYMV-ZZ and six other isolates (Table 3). The nucleotide sequence identities for the individual ORFs and UTR of RNA1 between WYMV-ZZ and six other isolates were 98.0 to 99.0% for P3, 96.5 to 98.5% for 7K, 95.5 to 97.7% for CI, 93.5 to 96.7% for 14K, 96.4 to 98.9% for NIa-VPg, 96.1 to 97.1% for NIa-Pro, 96.9 to 97.5% for CP, 96.6 to 97.7 for 5′ UTR and 96.5 to 98.1% for 3′UTR; for the individual ORFs and UTR of RNA2 the nucleotide sequence identities between WYMV-ZZ and six other isolates were

Table 2. GenBank accession numbers of seven WYMV isolates.

Isolate	Place	RNA1	RNA2
WYMV-HC	Huangchuan, Henan Province	AF067124	AF041041
WYMV-YZ	Yangzhou, Jiangsu Province	AJ131981	AJ131982
WYMV-YA	Yaan,Sichuan Province	AJ239039	AJ242490
WYMV-ZMD	Zhumadian, Henan Province	FJ361766	FJ361769
WYMV-XQ	Xiaqiao, Jiangsu Province	FJ361764	FJ361767
WYMV-ZZ	Zhouzhi, Shanxi Province	FJ361765	FJ361768
WYMV-JPN	Japan	D86634	D866350

94.9 to 98.3% for P1, 93.8 to 98.3% for P2, 91.1 to 98.2% for 5′ UTR, and 98.2 to 99.0% for 3′ UTR. At the amino acid level, the identities for the individual ORFs of RNA1 between WYMV-ZZ and six other isolates were 96.6 to 98.8% for P3, 95.5 to 98.5% for 7K, 93.9 to 97.6% for CI, 91.9 to 97.6% for 14K, 93.0 to 98.9% for NIa-VPg, 90.0 to 97.3% for NIa-Pro, and 98.0 to 98.6% for CP; for RNA2 the identities were 94.5 to 98.8% for P1 and 94.0 to 98.0% for P2.

Phylogenetic analysis of seven different isolates

To better understand the relationship between WYMV-ZZ and six other isolates, the phylogenetic analysis of seven different isolates was constructed. Phylogenetic trees were constructed for P3, 7K, CI, 14K, NIa-VPg, NIa-Pro, CP, and full-length of RNA1, and for P1, P2, and full-length of RNA2 by the neighbor-joining method and visualized using MEGA (version X) with 1000 bootstrap replicates. The results showed that P3, CI, 14K, NIa-VPg, NIa-Pro, NIb and CP of WYMV-ZZ were more closely related to WYMV-YA, 7K of WYMV-ZZ was close to WYMV-XQ; and that P1 and P2 of WYMV-ZZ were close to WYMV-ZMD (data not shown). The full-length of WYMV-ZZ was close to WYMV-YA for RNA1 and was close to WYMV-ZMD for RNA2 (Figure 2A and B). The phylogenetic trees generated based on the NIa-VPg region of RNA2 showed that this region clustered together with the other five Chinese isolates, while WYMV-JPN formed a distinct branch (Figure 2C and D).

Recombination analysis

The seven sequences of WYMV isolates were processed and examined for recombination at the same time. The major parent, minor parent, the event and the corresponding *P*-value of four recombination events are as shown in Figure 3 and Table 4. The most possible one recombination event of WYMV-ZZ, which is located in 2,598 to 4,019 nt of RNA1 CI region, may recombined with unknown major parent (WYMV-JPN) and minor parent (WYMV-HC) with a RDP *P*-value of 8.526×10^{-06}. The second recombination event of WYMV-HC, which is located in 564 to 894 nt of RNA2 P1, may recombined with major parent (WYMV-ZZ) and minor parent (WYMV-YA) with a RDP *P*-value of 5.444×10^{-05}. The third recombination event of WYMV-XQ, which is located in 1698 to 3196 nt of RNA P2 and 3′ UTR regions, may recombined with major parent (WYMV-ZMD) and minor parent (WYMV-YA) with a RDP *P*-value of 3.147×10^{-05}.

In this study, WYMV was detected in wheat leaves which is collected from Zhouzhi, Shanxi province of China in 2008. The wheat samples were infected with WYMV confirming by both RT-PCR and western blotting. For RT-PCR, targeting the VPg region in RNA1, primer VP-1M was used for reverse transcription reaction and primer pair VP-1P/VP-1M was used to amplify a 704 bp fragment; targeting the 3-termino-UTR in RNA2, primer ut-1M was used for RT reaction and primer pair ut-1P/ut-1M was used to amplify the 880 bp fragment. Using antiserum of WYMV-CP, Western blotting was carried out with the 32 kD positive band (Figure 1B).

Apart from short regions where the primers annealed at the 5'- and 3'-terminus, a nearly complete nucleotide sequence of WYMV-ZZ was determined and given the GenBank accession number FJ361765 for RNA1 and FJ361768 for RNA2, respectively (Table 2).

Based on the nucleotide sequence comparison, WYMV-ZZ shared 96.6 to 97.7% and 95.1 to 98.2% nucleotide sequence identity for RNA1 and RNA2 with the other six isolates (WYMV-HC, WYMV-YA, WYMV-YZ, WYMV-XQ, WYMV-ZMD, WYMV-JPN) infecting wheat in different parts of the world. At the amino acid level, WYMV-ZZ had 94.1 to 98.2% identity for RNA1 and 94.1 to 96.7% identity for RNA2 with other six isolates. The identity for genes of RNA1 and RNA2 were >90% between WYMV-ZZ and six other isolates (Table 3).

To better understand the relationship between WYMV-ZZ and other six isolates, the phylogenetic analysis were carried out using MEGA (version X) with 1000 bootstrap replicates. The results showed that P3, CI, 14K, NIa-VPg, NIa-Pro, NIb and CP of WYMV-ZZ were more closely related to WYMV-YA, 7K of WYMV-ZZ was close to WYMV-XQ; and that P1 and P2 of WYMV-ZZ were close

Table 3. Sequence identity comparison of WYMV-ZZ with other six isolates.

WYMV-ZZ	WYMV-HC		WYMV-YZ		WYMV-YA		WYMV-XQ		WYMV-ZMD		WYMV-JPN	
	nt (%)	aa (%)	nt (%)	aa (%)	nt (%)	nt (%)	aa (%)	aa (%)	nt (%)	aa (%)	nt (%)	aa (%)
A for full length												
RNA1	97.0	94.4	97.3	96.8	97.2	96.6	95.8	95.1	97.1	96.1	97.7	96.6
RNA2	96.9	96.7	97.3	96.5	95.1	95.9	94.1	96.1	97.0	96.5	98.4	98.2
B for coding region												
P3	98.9	98.5	99.0	98.5	98.3	98.0	96.6	98.8	98.8	98.2	99.0	98.2
7K	96.5	95.5	98.0	97.0	98.5	97.5	97.0	98.5	98.0	98.5	97.5	98.5
CI	96.4	96.1	96.7	95.6	96.8	95.5	93.9	97.6	96.7	95.8	97.7	97.1
14K	93.5	91.9	95.2	95.2	96.2	94.6	94.4	96.8	94.4	93.5	96.2	97.6
NIa-VPg	98.2	96.8	98.9	98.4	98.2	96.4	93.0	98.4	98.2	98.9	98.4	97.9
NIa-Pro	96.8	90.0	96.7	95.0	97.1	96.5	95.5	97.3	96.1	94.5	96.7	95.0
NIb	97.7	98.7	97.7	98.5	97.2	97.3	98.5	99.1	97.5	98.5	98.0	98.7
CP	97.2	98.0	97.4	98.3	97.3	97.5	98.6	98.6	96.9	98.0	97.5	98.6
5′UTR	97.0	-	97.3	-	97.2	96.6	-	-	97.1	-	97.7	-
3′UTR	98.1	-	97.3	-	98.1	96.5	-	-	97.7	-	97.7	-
P1	94.9	94.5	97.1	97.2	95.4	95.5	94.5	98.0	97.4	98.4	98.3	98.8
P2	97.0	97.5	96.8	96.1	93.8	95.1	94.0	95.4	96.2	95.7	98.3	98.0
5′ UTR	97.1	-	97.1	-	91.1	95.8	-	-	97.1	-	98.2	-
3′ UTR	98.7	-	98.7	-	99.0	98.2	-	-	98.7	-	98.8	-

to WYMV-YA for RNA1 and was close to WYMV-ZMD for RNA2 (Figure 2A and B). The phylogenetic trees generated based on the NIa-VPg region of RNA2 showed that this region clustered together with the other five Chinese isolates, while WYMV-JPN formed a distinct branch (Figure 2C and D).

Recombination of seven WYMV isolates was analyzed by RDP4.97. Six recombination detection methods were used to analyse putative recombinants and recombination breakpoints. The programs used were RDP, GENECONV, BOOTSCAN, MAXCHI, SISCAN and 3SEQ.

Detected by at least five different methods, three recombination events were received (Zhou et al., 2012). The recombination event detected in RNA1 CI region of WYMV-ZZ, which is located in 2,598-3,344 nt, may be recombined with unknown major parent (WYMV-YZ) and minor parent (WYMV-HC) with a RDP *P*-value of 8.526×10^{-06}. There was no recombination event RNA2 of WYMV-ZZ. Consistent nucleotide and amino acid, and close phylogenetic relationships may imply the molecular evolution of WYMV is a genetic stability progress.

DISCUSSION

The genomic RNA sequence of WYMV-ZZ was determined. Sequence comparison, phylogenetic tree and recombination analysis were performed among WYMV-ZZ and other six known WYMV isolates. Consistent nucleotide and amino acid, and close phylogenetic relationships may imply the molecular evolution of WYMV is a genetic stability progress.

VPg is a multiple function protein, which participates in the genomic replication and interacts with 3-terminal poly-A to achieve similar function with 5-terminal cap structure (Gallie et al., 1995; MURPHY et al., 1996; Ohshima et al., 2007). So far, there was little research about WYMV-VPg, the VPg of Potato virus Y exists in different forms to exercise different functions

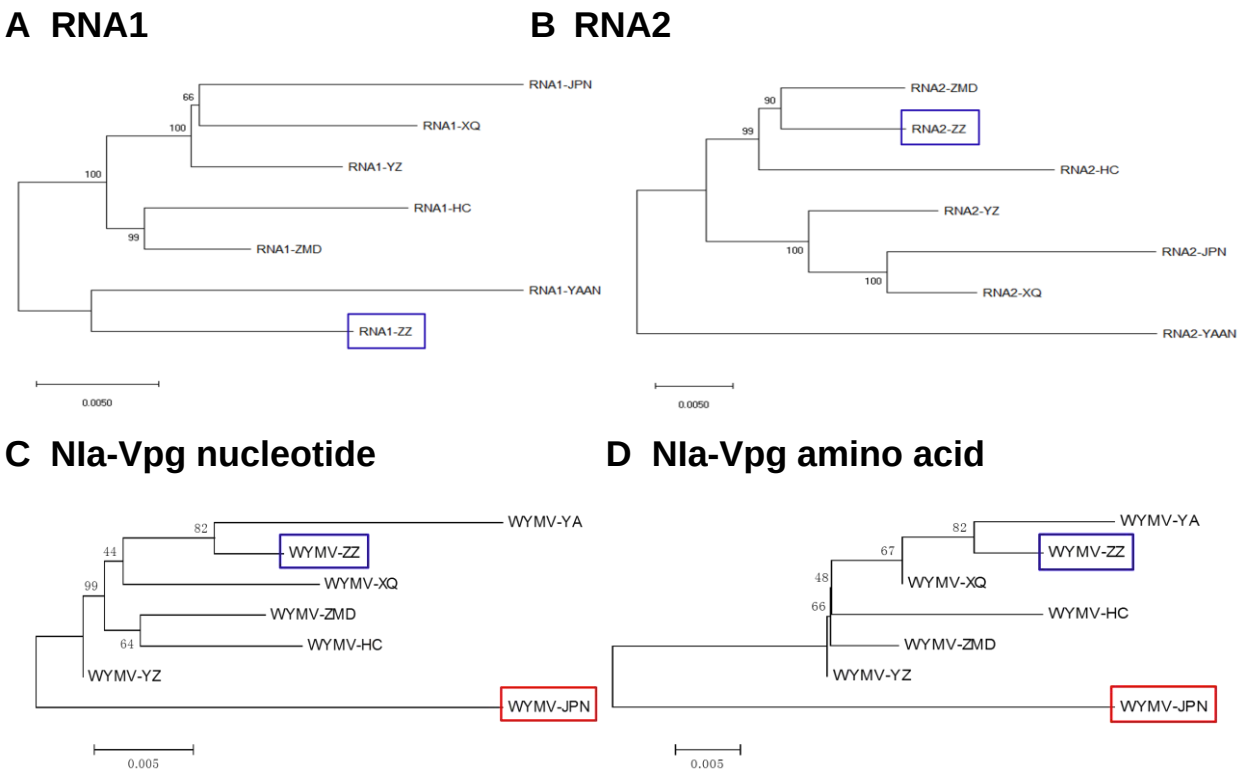

Figure 2. Phylogenetic trees generated by seven WYMV isolates. A, B: The phylogenetic trees for RNA1 and RNA2 nucleotide of seven WYMV isolates. Blue frame: WYMV-ZZ; C, D: Nucleotide and amino acid of VPg neighbor-joinging trees generated and the respective amino acid of seven WYMV isolates. Blue frame: VPg of WYMV-ZZ. Red frame: VPg of WYMV-JPN.

during the life cycle of virus. VPg of tobacco etch potyvirus is a host genotype-specific determinant for long-distance movement (Schaad et al., 1997; Daròs et al., 1999), and may also participate in inhibiting viral gene silencing (Germundsson et al., 2006). Sequences of VPg region were used for distinguishing two Japanese pathotypes (WYMVY-T and WYMV-M) (Ohto et al., 2005). Moreover, WYMV VPg accumulated in both the nucleus and cytoplasm of infected cells but exclusively localized in the nucleus when expressed alone in plants, and VPg interacted with WYMV coat protein (CP) and proteinase 1 (P1) proteins in vitro and in planta assays, WYMV-P1 may adjust to facilitate VPg activity through regulating VPg sub-cellular distribution (Rong, 2011). The structural and subcellular distribution of VPg protein was analysed that VPg protein contained a nuclear localization signal and a nuclear export signal, that VPg protein was detected in both cytoplasm and nucleus in virus infected leaves of wheat plant cells (Bian, 2013). In addition, the WYMV-Nib8 gene was trasformed into the transgenic wheat line N12-1, and this transgenic wheat can effectively control the wheat yellow mosaic virus disease (Fu et al., 2016).

Recently, the nucleotide sequences encoding CP and VPg of WYMV collected from five provinces of China was determined; the results showed the low level of genetic diversity and inferred that the WYMV in China was genetic stability or recent emergence (Sun et al., 2013). From this study, the seven WYMV isolates showed high sequence identity comparison with nucleotide and with amino acid and VPg may be the breakthrough point of WYMV ongoing molecular evolution.

CONFLICT OF INTERESTS

The authors have not declared any conflict of interests.

ACKNOWLEDGEMENTS

This research was supported in part by National Department Public Benefit Research Funds (201303021 and 2016ZX08002001) and partially supported by the Program for Changjiang Scholars and Innovative Research Team in University (IRT1042).

Abbreviations

WYMV, Wheat yellow mosaic virus; **WYMV-HC,** WYMV

A

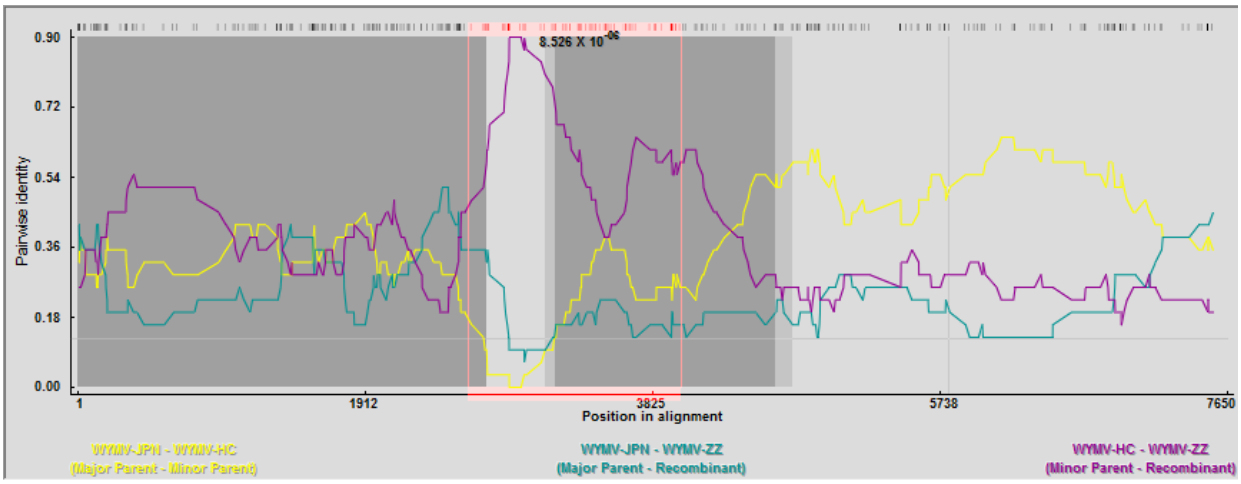

B

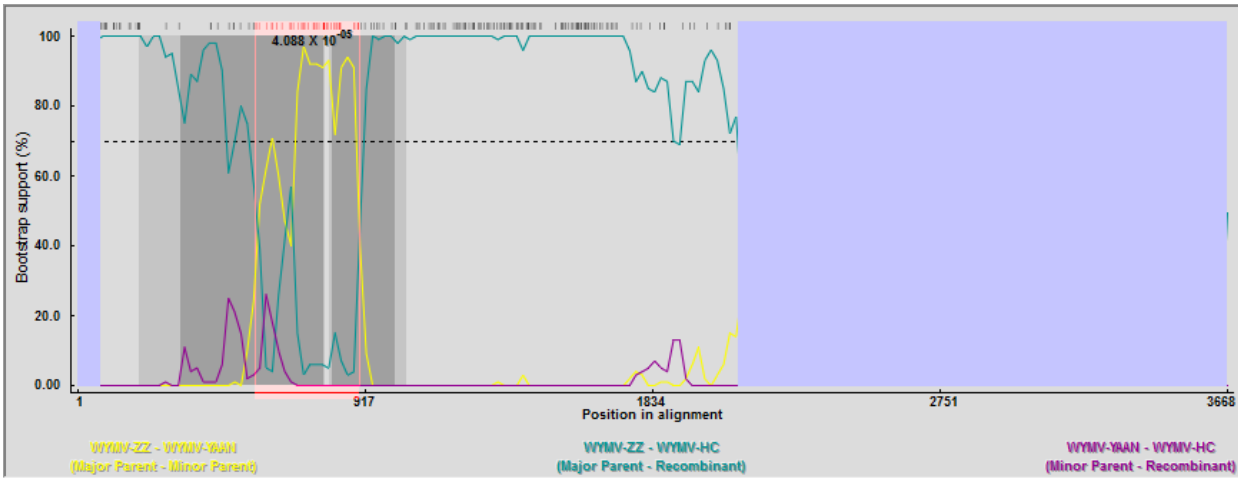

C

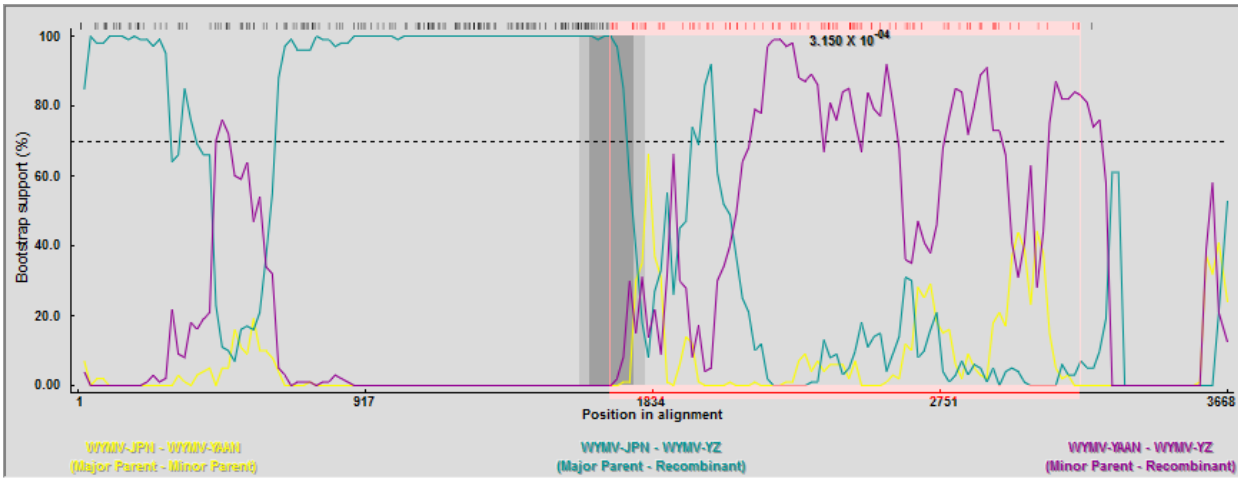

Figure 3. Recombination of WYMV analyzed using RDP4.97. A-D: BOOTSCAN plot for the recombinant of WYMV-ZZ within RNA1, of WYMV-HC within RNA2, and of WYMV-YZ within RNA2. The left and the right boundaries of the pink region indicate breakpoint positions. The yellow line is the major parent: minor parent plot, the green line is the recombinant plot; the dotted line indicates the bootstrap cut off value.

Table 4. Recombination events detected in WYMV isolates.

Event	RNA1	RNA2	RNA2
Recombinant	WYMV-ZZ	WYMV-HC	WYMV-YZ
Major parent	Unknown (WYMV-YZ)	WYMV-ZZ (98.4%)	WYMV-JPN (98.1%)
Minor parent	WYMV-HC (95%)	Unknown (WYMV-YAAN)	WYMV-YAAN (96.9%)
***P*-values determined using seven different programs**			
RDP	8.526×10^{-06}	$5.\times10^{-04}$	3.147×10^{-05}
GENECONV	1.031×10^{-06}	ND	ND
BootScan	3.214×10^{-08}	ND	3.150×10^{-04}
MaxChi	1.695×10^{-07}	2.601×10^{-04}	4.474×10^{-11}
Chimaera	9.839×10^{-06}	1.302×10^{-04}	2.923×10^{-09}
Siscan	2.500×10^{-08}	ND	4.204×10^{-05}
3Seq	1.901×10^{-03}	1.264×10^{-03}	2.041×10^{-08}
Beginning breakpoint (nt)	2598	564	1698
Ending breakpoint (nt)	4019	898	3196

ND: Recombination was not detected by this program.

isolate of Huangchuan, Henan province; **WYMV-YZ,** WYMV isolate of Yangzhou, Jiangsu province; **WYMV-YA,** WYMV isolate of Ya'an, Sichuan province; **WYMV-ZMD,** WYMV isolate of Zhumadian, Henan province; **WYMV-XQ,** WYMV isolate of Xiaqiao, Jiangsu province; **WYMV-JPN,** WYMV isolate of Japan; CP, coat protein; **VPg,** viral genome-linked protein.

REFERENCES

Chen J, Chen JP, Cheng YY, Diao A, Adams M J, Dua J (2000). Differences in cultivar response and complete sequence analysis of two isolates of wheat yellow mosaic bymovirus in China. Plant pathology 49(3):370-374.

Chen JP (1999). Molecular comparisons amongst wheat bymovirus isolates from Asia, North America and Europe. Plant pathology 48(5):642-647.

Chen WP, Chen PD, Liu DJ, Kynast R, Friebe B, Velazhahan R, Muthukrishnan S, Gill BS(1999). Development of wheat scab symptoms is delayed in transgenic wheat plants that constitutively express a rice thaumatin-like protein gene. Theoretical and Applied Genetics 99(5):755-760.

Clover G, Henry C (1999). Detection and discrimination of wheat spindle streak mosaic virus and wheat yellow mosaic virus using multiplex RT-PCR. European Journal of Plant Pathology 105(9):891-896.

Daròs JA, Schaad MC, Carrington JC (1999). Functional analysis of the interaction between VPg-proteinase (NIa) and RNA polymerase (NIb) of tobacco etch potyvirus, using conditional and suppressor mutants. Journal of Virology 73(10):8732-8740.

Fu W, Du Z, He Y, Zheng WJ, Han CG, Liu BF, Zhu SF (2016). Metabolic profiling of virus-infected transgenic wheat with resistance to wheat yellow mosaic virus. Physiological and Molecular Plant Pathology 96:60-68.

Gallie DR, Tanguay RL, Leathers V (1995). The tobacco etch viral 5′leader and poly (A) tail are functionally synergistic regulators of translation. Gene 165(2):233-238.

Germundsson A, Valkonen J (2006). P1-and VPg-transgenic plants show similar resistance to *Potato virus A* and may compromise long distance movement of the virus in plant sections expressing RNA silencing-based resistance. Virus Research 116(1):208-213.

Han CG, Li DW, Yu JL, Liu L, Shang QX, Liu Y (2002). Preparation and application of specific antiserum against *wheat yellow mosaic virus* coat protein expressed in *E. coli* cells. Journal of Agricutural Biotechnology 10(4):373-376.

Jin Y, Song JJ, Zhu TQ, Bai D, Wang HM (2016). Pathogen Identification of Wheat Yellow Mosaic Disease in Zhumadian Region and Evaluation of Wheat Cultivars Resistance. Journal of Henan Agricultural Science 45(3):87-91 http://www.hnnykx.org.cn/CN/abstract/abstract6778.shtml

Kumar S, Stecher G, Li M, Knyaz C, Tamura K (2018). MEGA X: Molecular Evolutionary Genetics Analysis across computing platforms. Molecular Biology and Evolution 35:1547-1549.

Li DW, Han CG, Xing YM, Tian ZF, Yu JL, Cai ZN, Liu Y (1997). Identification of the wheat yellow mosaic virus occurring in China by RT-PCR. Acta Phytopathol. Sinica 27(4):303-307.

Martin DP, Murrell B, Golden M, Khoosal A, Muhire B (2015). RDP4: Detection and analysis of recombination patterns in virus genomes. Virus Evolution 1(1):1-5.

Murphy JF, Klein PG, Hunt AG, Shaw JG (1996). Replacement of the tyrosine residue that links a potyviral VPg to the viral RNA is lethal. Virology 220(2):535-538.

Namba S, Kashiwazaki S, Lu X, Tamura M, Tsuchizaki T (1998). Complete nucleotide sequence of wheat yellow mosaic bymovirus genomic RNAs. Archives of Virology 143(4):631-643.

Ohshima K, Tomitaka Y, Wood JT, Minematsu Y, Kajiyama H,

Tomimura K, Gibbs AJ (2007). Patterns of recombination in turnip mosaic virus genomic sequences indicate hotspots of recombination. Journal of General Virology 88(1):298-315.
Ohto Y, Sakai JI (2005). The reassortment of genomic RNAs of Wheat yellow mosaic virus (WYMV) pathotype I and II in aresistant and a susceptible cultivar. Working Group on Plant Viruses with Fungal Vectors pp. 67-70.
Sawada E (1927). Wheat yellow mosaic prevention. Journal of Plant Protection 14:444-449.
Schaad MC, Lellis AD,Carrington JC (1997). VPg of tobacco etch potyvirus is a host genotype-specific determinant for long-distance movement. Journal of Virology 71(11):8624-8631.
Sun BJ, Sun LY, Tugume AK, Adamas MJ, Yang J, Xie LH, Chen JP (2013). Selection pressure and founder effects constrain genetic variation in differentiated populations of a soil-borne bymovirus Wheat yellow mosaic virus (Potyviridae) in China. Phytopathology 103(9):949-959.
Sun L, Bian J, Andika I B, Hu YC, Sun BJ, Xiang R, Kondo H, Chen JP (2013). Nucleo-cytoplasmic shuttling of VPg encoded by Wheat yellow mosaic virus requires association with the coat protein. Journal of General Virology 94(12):2790-2802.
Tao JF, Qin JZ, Xiao JH, Shen YZ, Zhao FZ, Li TJ, Xie YY, He DF, Rao YH, Huang XH (1980). Studies on the soil-borne yellow mosaic virus of wheat in Sichuan. Acta Phytopathology Sinca 10(1):15-27.
Wang H, Wu K, Liu Y, Wu Y, Wang X (2015). Integrative proteomics to understand the transmission mechanism of Barley yellow dwarf virus-GPV by its insect vector *Rhopalosiphum padi*. Scinece Report 5:10971
Yu JL, Yan LY, Su N, Hou ZJ, Li DW, Han CG, Yang LL, Cai ZN, Liu Y (1999). Analysis of nucleotide sequence of wheat yellow mosaic virus genomic RNAs. Science in China Series C: Life Sciences 42(5):554-560.
Zhang ZY, Xu JM, Han CG, Li DW, Yu JL (2010). Detective and complete sequence analysis of wheat yellow mosaic virus from Zhumadian in Henan Province. Acta Agricutural boreali-sinica (2):5-11.
Zhang ZY, Liu XJ, Li DW, Yu JL, Han CG (2011). Rapid detection of wheat yellow mosaic virus by reverse transcription loop-mediated isothermal amplification[J]. Virology Journal 8(1):550.
Zhou CJ, Xiang HY, Zhuo T, Li DW, Yu JL, Han CG (2012). Nucleotide sequence of a chickpea chlorotic stunt virus relative that infects pea and faba bean in China. Archives of Virology 157(7):1393-1396.

Related Journals: